Michael Tüchler, B.Sc.

Thiopyridazine based scorpionate complexes with zinc and iron for bioinorganic modelling

MASTERARBEIT

zur Erlangung des akademischen Grades

Master of Science

Masterstudium Chemie

eingereicht an der

Technischen Universität Graz

Betreuerin

Univ.- Prof. Dr. Nadia C. Mösch-Zanetti

Anorganische Chemie
Karl-Franzens-Universität Graz

Graz, Juni 2014

EIDESSTATTLICHE ERKLÄRUNG

AFFIDAVIT

Ich erkläre an Eides statt, dass ich die vorliegende Arbeit selbstständig verfasst, andere als die angegebenen Quellen/Hilfsmittel nicht benutzt, und die den benutzten Quellen wörtlich und inhaltlich entnommenen Stellen als solche kenntlich gemacht habe. Das in TUGRAZonline hochgeladene Textdokument ist mit der vorliegenden Masterarbeit identisch.

I declare that I have authored this thesis independently, that I have not used other than the declared sources/resources, and that I have explicitly indicated all material which has been quoted either literally or by content from the sources used. The text document uploaded to TUGRAZonline is identical to the present master‘s thesis.

Datum / Date

Unterschrift / Signature

Acknowledgement

First of all, I would like to thank my supervisor Prof. Dr. Mösch-Zanetti for the opportunity to work in her group and the interesting topic of the thesis. Despite her limited time, she always had an open ear for me and helped me with numerous of questions.
Additionally I would like to express my gratitude to Ass-Prof. Dr. Jörg Schachner. Thank you for the late night "sit-togethers" and your help with all the results, that did and did not make sense. Thank you for teaching me to re-question my results and preventing me from jumping into conclusions.
I would also like to thank Dr. Ferdinand Belaj for the X-ray measurements and the patience with me, all the time I thought I might have a crystal and for trying even the smallest needles. I am also grateful to Ing. Bernd Werner and Prof. Dr. Klaus Zangger for the NMR measurements and to Prof. Dr. Robert Saf for the high-resolution mass measurements.
I would also like to thank our lab technician Doris for her patience and helpfulness, all the time I needed new glass ware or chemicals. Furthermore, I would like to thank my lab colleagues for their patience with me and the fruitful discussions. Special thanks belongs to Natascha and Kathi for letting me use their hard – synthesized precursors.
Finally I would like to thank my girlfriend and my family. Thank you for showing me, that there is something else besides chemistry, so I could relax after a long working day. I am deeply indebted to my mother, who continuously supported me and therefore made it possible to complete this work and come so far.

Abstract

The sodium salt of the thiopyridazine based scorpionate ligand Na[Tn^{tBu}] (**1**) was synthesised by the reaction of 6-tert-butyl-3-thiopyridazine (**PnH**) with $NaBH_4$. A screening on the reaction conditions revealed that refluxing a 2.0 M solution of **PnH** with 1 equivalent of $NaBH_4$ in toluene for 2 days leads to 85% yield. The ligand is best purified via a reversed soxhlet extraction with cyclohexane.

Furthermore, it was found, that **1** is sensitive towards light and undergoes rapid decomposition upon UV - irradiation. The decomposition products were identified as **PnH** (2 equivalents) and 1 equivalent of the reduced 4,5- dihydro- 6- tert butyl- 3- thiopyridazine. Reaction of **1** with zinc halides in THF in the dark leads to the THF - coordinated complexes of the formula [ZnBr(Tn^{tBu})(THF)] (**3a**) and [ZnI(Tn^{tBu})(THF)] (**4**), respectively. Upon crystallization, **3a** loses its coordinated THF and a blue, scorpionate complex [ZnBr(Tn^{tBu})]$_6$ (**3b**) forms. X-ray diffraction analysis of **3b** reveals a hexameric structure, where each sulfur atom coordinates a different zinc atom. The analogous zinc iodine species [ZnI(Tn^{tBu})] (**5**) was synthesised by reaction of **1** with ZnI_2 in CH_2Cl_2. The complexes were characterised by ^{1}H and ^{13}C NMR spectroscopy, IR spectroscopy and high resolution mass spectrometry.

The hybrid Na[^{Pn}Bm] scorpionate ligand, consisting of two thiomethimidazoles and one thiopyridazine, reacts with zinc bromine to form a bidentate, dimeric complex of the formula [ZnBr(^{Pn}Bm)]$_2$ (**6**). X-ray diffraction analysis revealed, that two zinc atoms are bridged via the scorpionates thiopyridazine substituent. Furthermore, a weak B-H-Zn interaction is observable. ^{1}H and ^{13}C NMR spectroscopy, IR spectroscopy and elemental analysis confirmed the structure and purity of the compound.

An iron(II) scorpionate complex (**7**) was synthesised, reacting **1** with iron(II)triflate in Et_2O under inert atmosphere. Characterisation via IR spectroscopy and high-resolution mass indicate a complex of the putative formula [Fe(Tn^{tBu})(OTf)]. NMR measurements point to a paramagnetic compound and the IR spectrum shows a strongly shifted B-H resonance.

Reaction of **PnH** with $Fe(OTf)_2$ leads to formation of an unusual, trisulfide bridged, N,S,N - coordinating Fe(II) complex $[Fe(PnS_3Pn)_2](OTf)_2$ (**8**). The complex shows strong paramagnetic properties and measurements on a Gouy balance revealed a magnetic susceptibility, consistent with a high spin complex with 4 unpaired electrons. The complex was characterised via IR spectroscopy and elemental analysis. X-ray diffraction analysis of **8** revealed an octahedrally coordinated Fe(II) center with two facially coordinating, tridentate ligands.

Abbreviations

Abs	Absorption
ACN	Acetonitrile
Ar	Aryl
Asp	Aspartic acid
Bim	Benzimidazole
CarO	Carotene Oxygenase
$CDCl_3$	Deuterated chloroform
CDO	Cysteine dioxygenase
Cys	Cysteine
DCM	Dichloromethane
DKE	Diketo dioxygenase
DMSO	Dimethylsulfoxide
Glu	Glutamic acid
His	Histidine
HSAB	Hard and soft acids and bases
IR	Infrared (spectroscopy)
MeOH	Methanol
Mim	Methimidazole
MW	Microwave
NADH	Reduced form of nicotinamide adenine dinucleotide
NHIE	Non-heme iron containing enzymes
NMR	Nuclear magnetic resonance (spectroscopy)
^{Pn}Bm	3-thiopyridazinyl - bis(2-mercapto-methimidazolyl) borate

Py	Pyridine
Pn	Pyridazine
QDO	Quercetin dioxygenase
SyrB2	Halogenase
tBu	Tertiary butyl group
THF	Tetrahydrofurane
Thr	Threonine
Tm	Tris (2-mercapto-methimidazolyl) borate
Tn	Tris (3-thio-pyridazinyl) borate
Tp	Tris (pyridazinyl) borate
Tyr	Tyrosine
UV	Ultra violett (light)

Contents

Chapter 1.

Introduction: Zinc and iron in biology

1.1. Zn-dependent enzymes

Due to its full d-shell, zinc lacks a lot of abilities, that makes other metals more interesting for organometallic and catalytic chemistry. In contrast to copper, iron or manganese, zinc neither possesses colour, nor redox activity or magnetism and its oxidation state is limited to +2, which excludes its complexes from classic catalysis. Despite its limited properties, the zinc metal has a lot of functions in living organisms. An average adult human contains about 3 g of zinc, which is responsible for effective growth and development.[1,2] Furthermore it is proposed, that it shortens the length of a common cold in adults.[3–5] These effects are due to its catalytic and structural roles in enzymes and thus, there are zinc enzymes known for all fundamental enzyme classes like oxidoreductases, transferases, hydrolases, lyases, isomerases and ligases.[6,7]

1.1.1. Coordination motives in mononuclear zinc enzymes

Generally, the active site in zinc dependent enzymes consists of a tetrahedral zinc center, coordinated by 3 of the proteins amino acids and a catalytically important water molecule

or hydroxide ion.[8–12] The bound amino acids are usually a combination of histidine (His), aspartic acid (Asp), glutamic acid (Glu) and cysteine (Cys), respectively. Figure 1.1 shows the amino acids that provide nitrogen, oxygen and sulfur donors, being histidine one of the most common.[13–15]

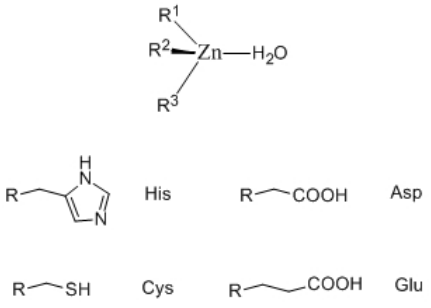

Figure 1.1.: different coordination motives and amino acids.

Histidine represents a neutral ligand coordinating with its imidazole-nitrogen atom, while the aspartic- and glutamic acid are deprotonated and coordinate via their carboxylic group. In contrast to these amino acids, the protonation state of the bound cysteine is under discussion. Some calculations suggest, that most probably all cysteine is bound by its deprotonated form, especially in the presence of other stabilizing amino acids.[16,17]

Although tetrahedral zinc centers are often quite similar concerning their coordination geometry and ligands, they perform different functions. This is believed to be due to different combinations of donor groups and different lengths of the spacer between the amino acids and the coordinating residues. This generates an active site, which is perfectly adapted for the respective function.[18]

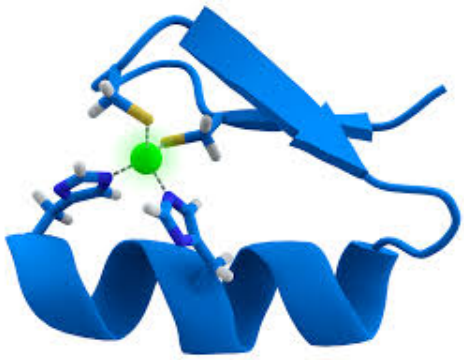

Figure 1.2.: scheme of a zinc finger motive.

Additionally to their catalytic function, zinc enzymes play an important structural role, because they have a huge impact on the conformation and stability of enzymes. Other than in catalytic zinc enzymes, in structural sites, the cysteine is predominant. In structural sites, nitrogen and sulfur donors are favoured. This is illustrated by the $[Zn(Cys)_4]$ and the $[(His)_2(Cys)_2Zn]$ motive in Alcohol Dehydrogenase and the zinc finger, respectively (Figure 1.2).[19–21]

1.1.2. Carbonic anhydrase

Upon all zinc enzymes, the carbonic anhydrase is probably one of the most investigated.[22–24] Discovered in 1933, it was the first known zinc-containing enzyme and it was found, that it is ubiquitous (is present in animals, plants and bacteria).[25] The intense investigation of this enzyme derives from its unique catalytic function: the reversible hydration of carbon dioxide to bicarbonate. Thus it is important for respiration, CO_2 transport and the intracellular CO_2/HCO_3^- equilibrium.

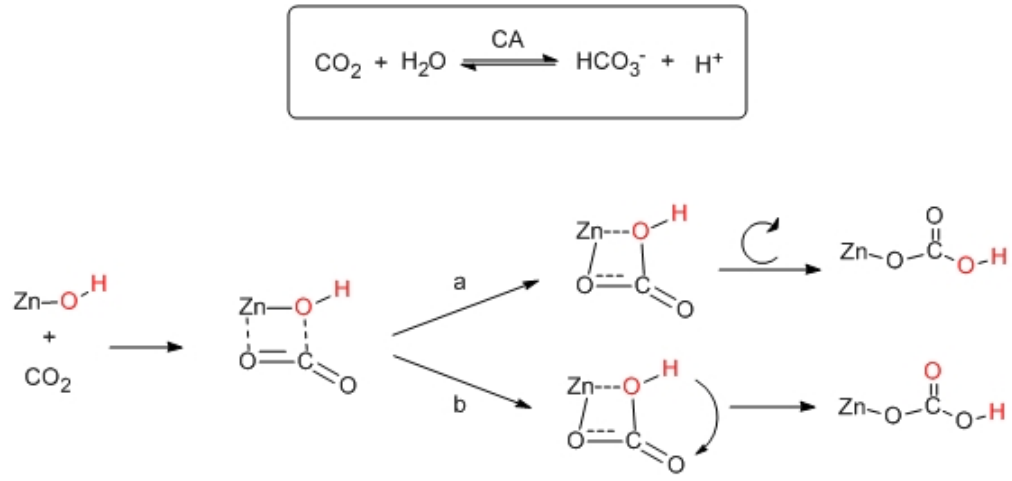

Figure 1.3.: proposed mechanism of carbonic anhydrase.

There have been several theoretical and experimental studies that investigated the mechanism of carbonic anhydrase.[26,27] In figure 1.3, the proposed mechanism based on these studies is illustrated. Starting with the deprotonation of the bound water, the catalytically active Zn-OH species is formed. After a nucleophilic attack of the Zn-bound hydroxide, a 4-membered intermediate is formed. From this intermediate, two possible pathways are possible. The "Lindskog" mechanism (Path a) and the "Lipscomp" (Path b) vary by the positioning of the originally zinc bound oxygen atom (red). While the "Lipscomp" mechanism is based on an internal proton transfer, the "Lindskog" mechanism goes with an unbroken O-H bond. Although it is not possible to experimentally observe these species and therefore confirm one of these mechanisms, some theoretical studies support a Lindskog-type mechanis.[28–30]

In order to successfully model the carbonic anhydrase, the structure and coordination around the active center is of particular interest.

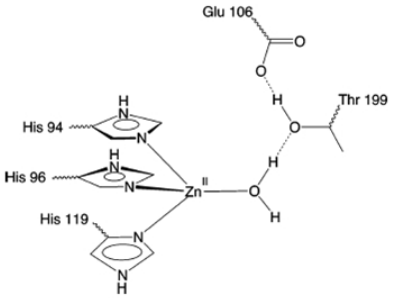

Figure 1.4.: active site of CA.

Figure 1.4 illustrates the tetrahedral zinc center, facially coordinated by 3 histidine, while the 4^{th} site is occupied by a water molecule. The water again is stabilized via hydrogen bonds to a threonine (Thr) and a glutamic acid (Glu). In the deprotonated form, the hydroxide can be stabilized by a hydrogen bond from Thr.

1.1.3. Modelling of the carbonic anhydrase

Illustrated in figure 1.4, the active center of the carbonic anhydrase can be modelled by a tetrahedral zinc-hydroxide complex. Naturally, the use of simple pyridazines or imidazoles leads to the formation of a tetrahedral $[ZnL_4]^{2+}$ and an octahedral $[ZnL_6]^{2+}$ complex and no zinc-hydroxide or zinc-aqua complex could be isolated so far.[31] Therefore, tripodal ligands, where the donating groups are attached to a common tetrahedral center have proven to be good ligands (Figure 1.5). In contrast to acyclic ligands, they enforce a facial coordination rather than a planar T-shaped binding. The facial coordination is required to generate a tetrahedral metal center. Furthermore, tripodal ligands are not very flexible and therefore can only coordinate in one binding conformation. This is also an important factor for modelling an enzymes active site.

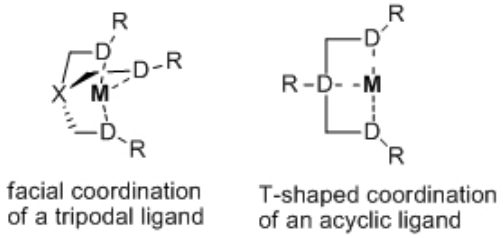

Figure 1.5.: coordination of a tripodal and an acyclic ligand.

Additionally, by varying the residues of the tripodal ligands, the steric environment around the metal center can be varied easily to generate a suitable coordination pocket.

Therefore, a variation of different tripodal ligands containing nitrogen donors have been applied to generate synthetic analogues of the carbonic anhydrase active center. A lot of effort was put into tris(imidazolyl)phosphine, tris(imidazolyl)carbinol or tris(imidazolyl)alkane ligands and their pyrazole derivatives, but only a few of them afforded a tetrahedral zinc complex.[32–39]

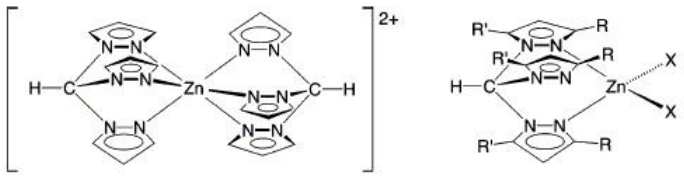

Figure 1.6.: sandwich- and bidentate coordinating zinc complexes.

Figure 1.6 shows the first structurally characterized zinc-complexes derived from tris-(pyrazolyl)methane ligands. But instead of a tetrahedral zinc complex, they form a sandwich-type complex of the formla $\{[\eta^3 - HC(L_3)]_2 Zn\}^{2+}$ and $\{[\eta^3 - HOC(L)_3]_2 Zn\}^{2+}$, respectively.[40] Furthermore, the increase of steric hindrance using highly substituted tris(pyrazolyl)methane ligands did not lead to the desired mononuclear cationic zinc species. Instead these ligands formed six-coordinated complexes of the formula $[\eta^3 - HC(L)_3]Zn(NO_3)_2$ and tetrahedral, bidentate coordinated halide derivatives of the formula $[\eta^2 - HC(L)_3]ZnX_2$.[41]

The first ligand to form a tetrahedral zinc hydroxide complex was Trofimenko´s tris (pyrazolyl) borate scorpionate ligand [Tp].[42,43]. Since that, a lot of effort was put into the development of zinc scorpionate complexes. Figure 1.7 shows the first functional model, that was able to insert CO_2 into the Zn-OH bond, generating a zinc-bicarbonate complex.[44] The resulting complex however, does not exchange the bicarbonate with a hydroxide to restart a new cycle but rather condensates with a zinc hydroxide forming a carbonato-bridged dimer.[45]

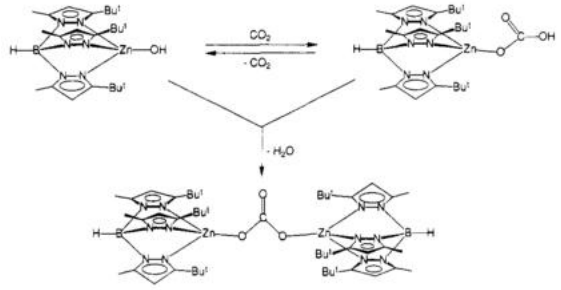

Figure 1.7.: the first functional model of carbonic anhydrase.

In 1996, Reglinski et al. introduced another class of scorpionate ligands. His 2-mercapto-methimidazole - based scorpionate [Tm] was able to bind via its sulfur atom and therefore generating an 8- membered ring, that is more flexible than the original [Tp] ligand.[46] Based on this new ligand, Bridgewater et al. were able to characterize a stable S^3-coordinating zinc-hydroxide complex (Figure 1.8A).[47]

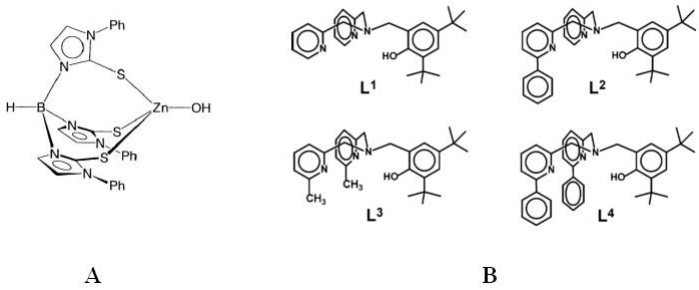

Figure 1.8.: A: S^3-coordinating Zn-OH complex B: N-based scorpionates.

The first non-boron based tripodal ligands, that form zinc-hydroxide complexes were introduced in 2005 by Vahrenkamp et al. (Figure 1.8B). These nitrogen based ligands generate a tetrahedral zinc-aqua complex and with highly sterical substituents (L4), a zinc complex with a vacant site is formed.[48]
With the introduction of mixed hybrid scorpionates, the field of research in the zinc-scorpionate chemistry widened up.[49] In 1997, Kimblim et al. successfully characterized a zinc halide complex with a bis(2-mercapto-methimidazolyl)pyrazolyl borate ligand (Figure 1.9).

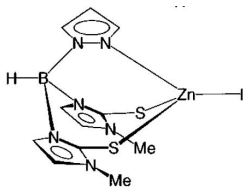

Figure 1.9.: first mixed scorpionate complex.

In 2003, Shu et al. showed, that also sterically encumbered mixed bis(2-mercapto-methimidazolyl) pyrazolyl borate ligands do not form a Zn-OH species but undergo decomposition upon hydrolysis.[50]
Other classes of scorpionate ligands were introduced and applied in this field, like the pyridine-based-[51] or the triazole-based scorpionates[52] but none of them showed better results, than the original Tp ligand.

1.2. Fe-dependent enzymes

Iron is the most abundant element in the earth crust and the human body contains about 4-5 g iron, of which approximately 50% is bound in hemoglobin.[53] Furthermore, it has several stable oxidation states, varying from the common +2 and +3 to high valent +4 and +5 in active intermediates in non-heme iron containing enzymes (NHIEs).[54,55] Due to its different oxidation states and coordination geometries, iron catalysts find a lot of application in industrial processes.[56]

In nature, iron has several important functions. In blood, for example, iron is coordinated by a heme-motive building the hemoglobin, which is responsible for oxygen transport. Because of the fact, that iron is easily available and there are a lot of iron dependent enzymes, there is a huge interest in the field of iron chemistry.[54–58]

1.2.1. O_2 activation of non-heme Fe enzymes

In enzymes bearing a heme-iron motive (Figure 1.10), the iron center is coordinated by 4 nitrogen atoms of a planar porphyrin cofactor.

In this iron-porphyrin complex - like in hemoglobin, the iron center is additionally coordinated by a sulfur from cytochrome P450, leaving one vacant, active site. As a consequence, no other substrate can bind and thus NADH is necessary for reduction and a reductase is required for electron transfer.[58]

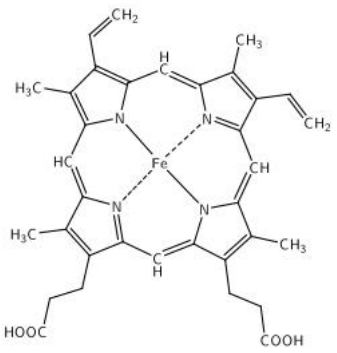

Figure 1.10.: Fe-porphyrin complex.

Non-heme iron containing enzymes (NHIEs), on the contrary, possess a lot of electron sources like co-factors or bound substrates. Therefore, they have a more flexible coordination environment to bind the various required ligands. Thus, NHIEs can catalyse a broad set of oxygen dependent transformations like oxygenative bond cleavage, bond formations or hydroxylations.[58] Although the functions are different, the enzymes share the common catalytic principle.

Figure 1.11 shows the general schematic mechanism of O_2 dependent transformations catalysed by NHIEs. ***A:*** The substrate binds to the active site, releasing H_2O. ***B:*** Oxygen binds end-on to the activated iron-substrate complex. ***C:*** The enzyme-dependent transformation is carried out, releasing the oxidised substrate and re-coordinating water to finish the catalytic cycle.[55]

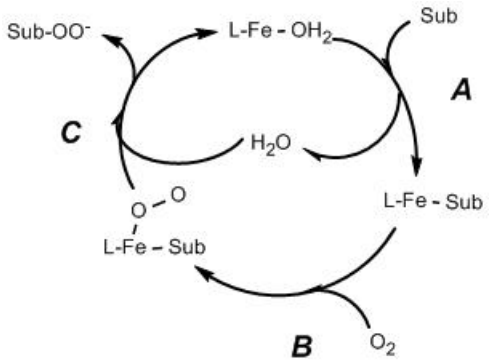

Figure 1.11.: general mechanism of O_2 activation by NHIEs.

With the first crystal structures of non-heme iron(II) containing enzymes, a trend in the coordination sphere was observable.[59,60] This coordination motive - referred as 2His-1-carboxylate facial triad - is illustrated in figure 1.12. It consists of 2 N-coordinating histidine, a carboxylic acid - based amino acid and a water molecule providing a 2N2O coordination.

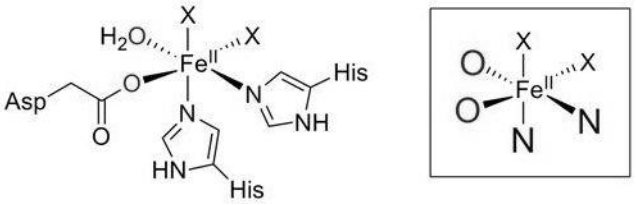

Figure 1.12.: 2His-1-carboxylate facial triad.

This facial triad has long been a paradigm for Fe(II)/Fe(III) active sites and numerous of ligands and complexes have been synthesised forming structural and functional models.[61–66] But by the time, new crystal structures of NHIEs emerged, that showed different coordination motives (Table 1.1).[67,68]

enzyme	name	motive
QDO	Quercetin dioxygenase	3His-1Glu
DKE	Diketo dioxygenase	3His
CDO	Cysteine dioxygenase	3His
SyrB2	Halogenase	2His-1Cl
CarO	Carotene oxygenase	4His

Table 1.1.: list of different motives in NHIEs.

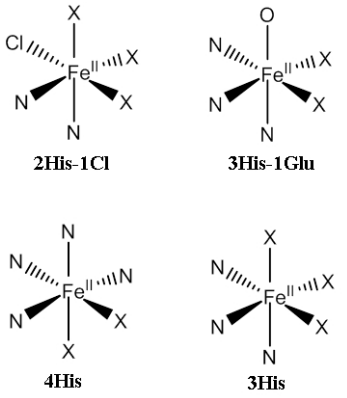

Figure 1.13.: different motives of NHIEs.

The new motives listed in table 1.1 differ in many ways compared to the "old" 2His-1-carboxylate" motive. The unusual 2His-1Cl motive, found in the halogenase enzyme, shows a chlorine bound to the active site and 3 vacant, solvent occupied sites. The 3His-1Glu motive is similar to the 2His-1-carboxylate motive, but is now coordinated by 3 nitrogen atoms (instead of 2) and one oxygen (instead of 2). Cysteine dioxygenase and Diketo-dioxygenase show a 3His and a 4His motive, respectively. In these enzymes, the iron center is coordinated only by nitrogen atoms, leaving 2 and 3 vacant, solvent occupied sites for the oxygen and the substrates to bind.

Figure 1.14 shows the different reactions catalysed by DKE1, CDO and QDO. The latter catalyses the oxygenative bond cleavage of quercetin and quercetin related structures,[69] while DKE1 was found to cleave α - diketones.[70] Cysteine dioxygenase oxidises cysteine forming cysteine-sulfinic acid.[71]

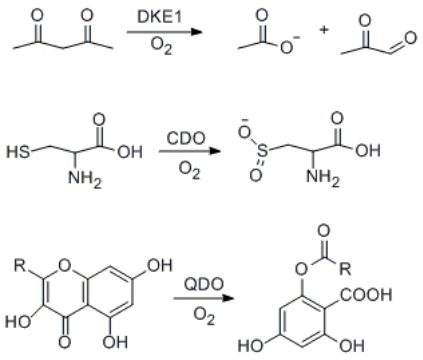

Figure 1.14.: reactions catalysed by different NHIEs.

1.2.2. CDO - cysteine dioxygenase

The cysteine dioxygenase, as mentioned before, catalyses the O_2 dependent conversion of L-cysteine into L-cysteinesulfinic acid (Figure 1.14). The enzyme is present in mammalian cells, as well as in yeast and prokaryotic homologues.[72] Numerous studies, including metal dissociation experiments, showed, that the enzyme is strictly Fe-dependent and requires a tyrosine (Tyr) co-factor.[71,73]

The structure of the active site (seen in figure 1.15 and 1.13) consists of a facial triad of N-coordinating histidine, while the fourth site is occupied by a water molecule, resulting in a distorted tetrahedral geometry. The co-factor tyrosine stabilizes the Fe-OH_2 via hydrogen bonding. In the active state (seen in figure 1.15), the cysteine binds $\varepsilon - N$ and $\varepsilon - S$ to the iron center, raising the coordination number to 5.[71,74]

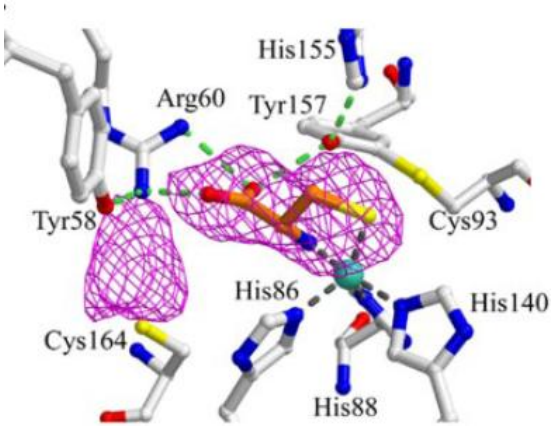

Figure 1.15.: active site of CDO.

A lot of effort was put into the determination of the catalytic mechanism and several studies have come up with the proposed mechanism, seen in figure 1.16. In the resting state, the center is tetrahedrally coordinated by 3 His and a water molecule (***A***). Cysteine replaces the water molecule by the S-atom and additionally coordinates via its nitrogen, forming a coordinately unsaturated complex (***B***). Next, O_2 binds end-on, which is stabilized by a hydrogen bond from the tyrosine co-factor (***C***). Without stabilisation, an oxoferryl species would form, releasing a hydroxyl-radical (***I***). Due to the close distance, a peroxo intermediate with the sulfur is proposed (***D***), followed by a homolytic cleavage of the O-O bond (***E***). The resulting oxoferryl species (again stabilized by the Tyr-cofactor) is known as a strong oxidising agent, and a S-O bond is formed (***F,G***). After reductive elimination (***H***) and hydrolysis, the cysteinesulfinic acid is released and the resting state is re-established (***A***).[71,74–78]

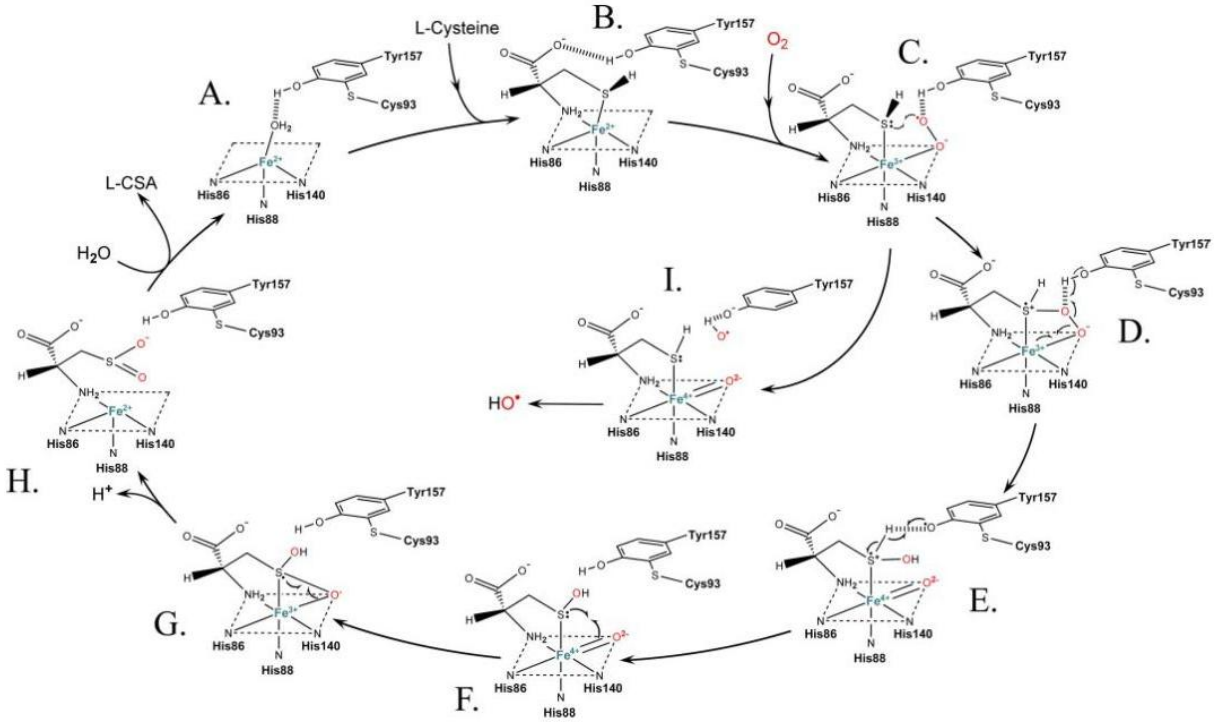

Figure 1.16.: proposed catalytic cycle of CDO.

Although different studies have come up with the proposed catalytic cycle, it has not been proved so far. In order to do so, numerous structural and functional models have been developed. In the beginning, the applied ligands were mainly amines with N-containing residues, shown in figure 1.17.

These ligands could be used in a tridentate (HNR_2) or a tetradentate (NR_3) manner with different N-coordinating residues like benzimidazole, pyridine or methimidazoles. Mixed ligands of these derivatives have also been reported.[79,80]

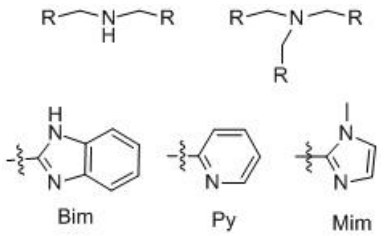

Figure 1.17.: N-based amine ligands.

Nevertheless, none of these purely nitrogen-containing ligands showed any activity towards oxygen activation. The first structural and functional models for CDO were reported by Goldberg and co-workers. In these studies, a new, sterically demanding pyridine based Schiff base ligand was introduced (Figure 1.18).[81] Using the N3-ligand with an equivalent

of NaS-Ph, the corresponding thiolate complex could be isolated. This complex was able to activate oxygen, forming a sulfinato-complex. With these ligands, it could be shown, that sulfur coordination is required for dioxygen activation. Furthermore, it was recognizable, that covalently bound sulfur-donors were over-oxidised to a R-SO_3 species.[82]

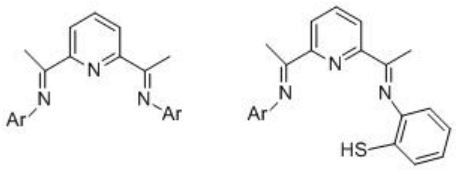

Figure 1.18.: pyridine Schiff-base ligands.

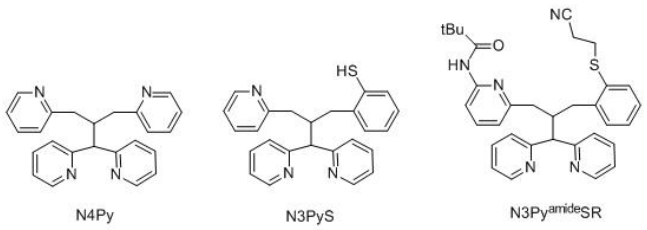

Figure 1.19.: N4Py ligands.

Introducing the N4Py ligands (Figure 1.19), Goldberg and co-workers were able to oxidise covalently bound S-donors (like in the N3PyS ligand) to the corresponding sulfinic acid. By varying the substitution of the ligand (like in the N3Py^{amide}SR ligand), the tyrosine co-factor could be modelled , which led to a spectroscopically characterized Fe(IV) oxo-ferryl species, using PhIO as oxygen source.[83]

Among all the previously described ligands, based on pyridine, imidazole, pyrole and benzimidazole, complexes with pyridazine containing ligands are still unexplored.

1.3. Thiopyridazine and its derivatives

Pyridazines and its substituted analogues are of particular interest, due to their versatile applications in biology. Not only do they interfere in several regulation processes in enzymes,[84–86] but they also show high biological activity and fungicide properties.[86,87]

1.3.1. Structural and chemical properties

Due to its electron deficient aromatic system, pyridazine and its derivatives show different behaviour in coordination chemistry, than other N-containing ligands. Compared to pyri-

dine, they have decreased electron donor abilities, which is demonstrated by their pK_A values (2.2 in pyridazine and 5.2 in the corresponding pyridine).[88]

Furthermore, bearing two vicinal nitrogen atoms would allow two metals to coordinate in close proximity to each other. However, this can only be achieved with 3- or 6- substituted pyridazines, where the residues bear coordinating atoms.[89,90] Unsubstituted, or alkyl-substituted pyridazines, instead, work as monodentate ligands, where only one metal binds.[91,92]

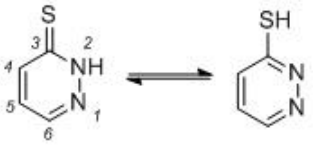

Figure 1.20.: tautomerism of thiopyridazine.

Substituting the pyridazines on the 3 - position with donor atoms like oxygen or sulfur leads to the pyridazine-3-one and the 3-thiopyridazine, respectively. These new ligands have two tautomeric forms, represented in figure 1.20. Typically, the pseudo-aromatic ring is preferred (left side), but upon UV-irradiation the equilibrium shifts to the right side and the aromatic thiol is formed.[93,94]

In coordination chemistry, the thiopyridazine has the possibility to act as a monodentate and bidentate ligand. Furthermore, by introducing a sulfur and a nitrogen donor, the thiopyridazine can act as a hard, as well as a soft ligand, according to Pearson´s HSAB concept.[95]

1.3.2. Thiopyridazine based complexes

Despite its various functions in biology and its promising properties in coordination chemistry, there are only a few examples of thiopyridazine based complexes. Several complexes of pyridazine-3-one derivatives have been reported, but the thiopyridazine ligand is a rare exception.[96,97] Only recently, a series of tin complexes bearing thiopyridazine ligands was published.[98] In these examples, the thiopyridazine coordinated bidentate via its 2 - N and S-atom, forming a planar 4-membered ring. Except for this example, no other

thiopyridazine - based complex has been described.

While there is only little known about thiopyridazine complexes, the ligand class of thiopyridine complexes is well established. There are examples of thiopyridine coordinating in a monodentate or in a bidentate fashion and in some cases, the thiopyridine serves as monodentate - bridging molecule, connecting two metal-complexes via its sulfur and nitrogen atoms (Figure 1.21).[99–101]

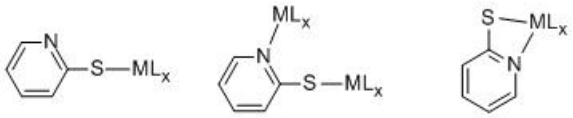

Figure 1.21.: different coordination modes of the thiopyridine ligand.

In zinc complexes, thiopyridines usually bind monodentate via their sulfur atom, but there are some rare examples of a bidentate thiopyridine zinc complex.[102,103] The coordination chemistry of iron thiopyridines depends on the co-ligand used. With strong coordinating ligands, like iron-nitrosyls, the thiopyridine is bound monodenate. Using weakly or non - coordinating ligands like carbonyls or $[PF_6]^-$, the iron is coordinated by the nitrogen and the sulfur in a bidenate manner.[104,105]

1.3.3. Thiopyridazine based scorpionates

While there are only a few complexes with thiopyridazines known, in 2011, Mösch-Zanetti and co-workers published a new, soft-coordinating, electron deficient scorpionate ligand based on 3-mercapto pyridazine (PnH).[106] This new potassium salt of the scorpionate ligand has different possibilities to bind to the metal center, as shown in figure 1.22. Because of the two donating atoms in the ligand, it is possible to coordinate via its sulfur or nitrogen atoms, depending on the "hardness" of the metal. Furthermore, mixtures of a N,S coordination could be conceivable.

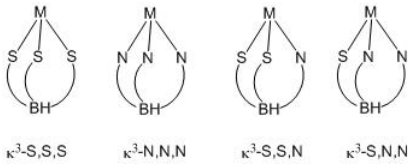

Figure 1.22.: different coordination modes of the scorpionate ligand.

Additionally, the coordination versatility of this scorpionate ligand is demonstrated by the crystal structure of the potassium salt of the tris(6-methyl-3-thiopyridazinyl)borate ligand (Figure 1.23).

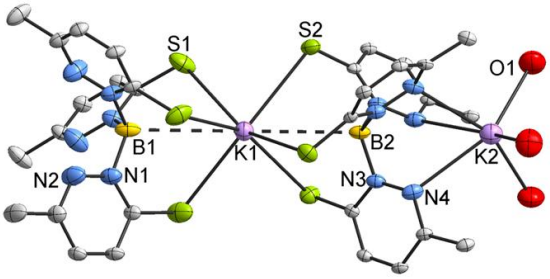

Figure 1.23.: crystal structure of $K[Tn^{Me}]$.

The ligand crystallizes as a dimer, forming a $\kappa^6 - S^6$ and a $\kappa^6 - N^3, O^3$ coordination, respectively. Interestingly, one potassium is coordinated only by sulfur atoms, while the other is surrounded by 3 nitrogen donors and 3 water molecules, providing an octahedral geometry.

Furthermore, the central boron of the scorpionate shows an inversion, indicating a beginning B-H-K interaction. With this electron deficient scorpionate ligand, unusual cobalt and nickel boratranes could be synthesised and characterized by X-ray crystallography.[106] These scorpionate derived boratrane complexes, first published by Owen and co-workers in 1999, are more stable, due to their closer ligand-metal distance.[107]

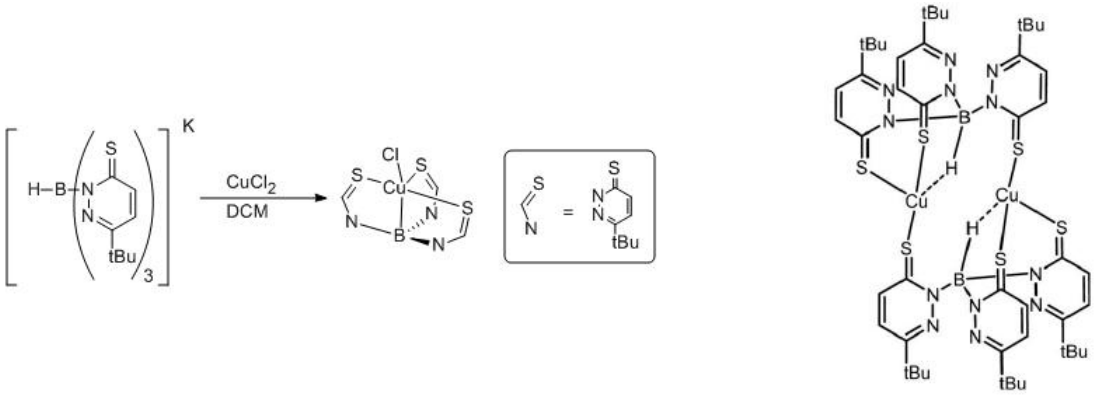

A B

Figure 1.24.: A: structure of a copper-boratrane, B: dimeric structure of $[Cu(Tn)]_2$.

Introducing this ligand to copper, the choice of solvent is crucial for the complex formation. While non-coordinating solvents like dichloromethane provide the copper-boratrane complex (Figure 1.24 A), coordinating solvents like THF or water form a dimeric $Cu_2[Tn]_2$ compound, seen in figure 1.24 B.[108] In this complex, one thiopyridazine-arm bridges two copper atoms. Furthermore the hydrogen atom at boron points to the copper center forming a Cu-H-B interaction.

1.4. Scope of the work

Because of the fact, that only the potassium salt of the thiopyridazine- based scorpionate ligand is known, this work focuses on the synthesis of the sodium- and thallium tris (6- tert butyl- 3- thiopyridazinyl) borate Na[Tn^{tBu}] and Tl[Tn^{tBu}] ligands, respectively. Furthermore, the best reaction conditions for the synthesis of the sodium salt were investigated (Figure 2.1).

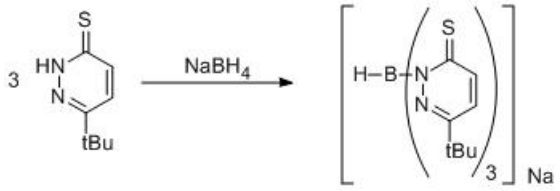

Figure 1.25.: synthesis of the ligand.

There was ample indication that, in contrast to K[Tn^{tBu}], the stability of the sodium salt Na[Tn^{tBu}] in solution is low. Thus, one goal of the work was to confirm the instability and to find conditions that allow using this ligand.

After finding the proper purification methods, the coordination behaviour of the ligand was to be tested towards zinc halides. The difference of the homo - thiopyridazine scorpionate and the hybrid thiopyridazine - thiomethimidazole scorpionate was analyzed.[109] Additionally, since only a few complexes with thiopyridazine ligands are known, the coordination behaviour of 6- tert butyl- thiopyridazine towards Fe(II) was investigated in order to obtain a better understanding of this unusual ligand and its better target-oriented use in future compounds.

Chapter 2.

Results and discussion

2.1. Synthesis of Na[Tn^{tBu}] (1)

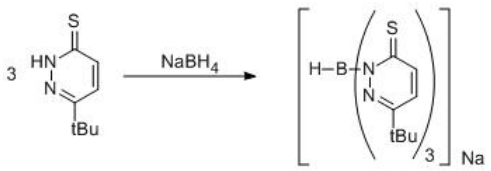

(2.1)

6-Tert-butyl-3-thiopyridazine [**PnH**] was used for the synthesis of the corresponding scorpionate ligand, seen in eq. 2.1. Under inert atmosphere, 1 equivalent of $NaBH_4$ and 3 equivalents of **PnH** were suspended and refluxed in toluene for 2 days. After cooling and triturating in pentane, the product was purified via reversed soxhlet extraction and dried in vacuo to obtain the product as a yellow powder in 85% yield. The ^{1}H-NMR spectrum of Na[Tn^{tBu}] (**1**) shows one singlet at 0.99 ppm, representing the tBu group, a broad singlet at 5.89 ppm for the B-H and two doublets at 6.99 ppm and 7.74 ppm representing the aromatic protons, respectively. In the IR spectrum of the compound, the B-H bond is apparent at 2536 cm^{-1}.

Scorpionates are commonly synthesised neat at high temperatures, however, the thiopyridazine decomposes under these conditions.[42] Therefore, a suitable solvent with a high boiling point had to be found.

2.1.1. Determination of the best reaction conditions

Originally, Nuss et al. synthesised the potassium salt of the ligand using diphenylmethane and 180°C.[106] For the sodium salt, different high - boiling solvents and the optimal reaction conditions for the synthesis were investigated. After a general reaction time of 2 days, the mixtures were filtered, washed with hot cyclohexane and dried in vacuo. All reactions were carried out under inert atmosphere, using fresh $NaBH_4$ stored in the Glove Box.

Table 2.1.: different solvents and stoichiometry.

Entry	solvent	stoichiometry	conversion
1	toluene dry	3:1	<5%
2	toluene	3:1	100%
3	toluene	4:1	100% *
4	xylene dry	3:1	0%
5	xylene (1% H_2O)	3:1	75%

* 1 equiv of PnH as side product

Table 2.1 summarizes the data obtained using various solvents and stoichiometry. The stoichiometry refers to the ratio between thiopyridazine and sodium borohydride. The data is discussed in the following sections.

Influence of the solvents water content

Clearly, the content of water in the solvent has a significant influence on the conversion. While dry toluene gives only very low yields (less than 5%), the use of bench top toluene leads to full conversion (Entries 1 and 2). Furthermore, the addition of 1% water to dry xylene increases the conversion from 0% to 75% (Entries 4 and 5).

Table 2.2.: different water content.

Entry	Equiv H_2O	conv.
1	0	0%
2	1	0%
3	2	>5%
4	3	>10%
5	4	0%

The conversion of compound 1 with different equivalents of water is listed in table 2.2. Using the parallel synthesiser, the effect of different water-concentrations on the reaction output was investigated. The resulting low conversions are probably due to the fact, that the reactions could not be carried out under inert atmosphere.

Comparison of the data from table 2.1 and table 2.2 shows, that both, an inert atmosphere and a water content of the solvent are crucial for the reaction. While a small water content is crucial for the reaction, high amounts of water or working not under inert atmosphere leads to a significant decrease of conversion. This might be due to decomposition of the $NaBH_4$ or disulfide formation of PnH.

Stoichiometry of the reaction

Incorrect stoichiometry could lead to bi- and tetrasubstituted boron species with the formula $[Pn_2BH_2]^-$ and $[Pn_4B]^-$, respectively. However, comparison of entries 2 and 3 in table 2.1 shows, that the influence of additional thiopyridazine is negligible. No $[Pn_4B]^-$ is formed and the additional equivalent, used in entry 3, can be found again in the product ratio of approx. 1:1, therefore yielding 100% conversion. This demonstrates, that additional thiopyridazine does not form any side-products or interferes with the scorpionate synthesis.

Influence of temperature

The conversion was not only determined after two days but was also followed by monitoring the evolution of H_2. By the use of a bubbler, the end of hydrogen evolution, and therefore the end of the reaction was observable. It was clearly visible, that the toluene-based reactions took more than a day to cease H_2 evolution, whereas the xylene based reactions were finished within 2-3 hours.

This led us considering using a microwave assisted synthesis. In this method, the reaction mixture is heated by MW - radiation. Because of the closed vessel and the resulting pressure, a solvent can be heated higher than its boiling point. Furthermore, the hydrogen evolution and therefore the reaction progress can be followed by measuring the increasing pressure (Figure 2.1).

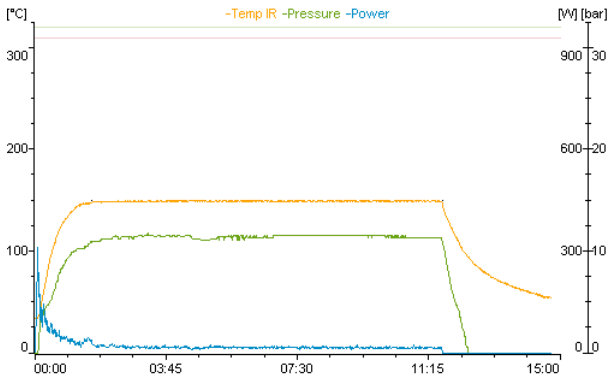

Figure 2.1.: reaction profile of the MW assisted synthesis of Na[Tn^{tBu}].

Using 3 mmol of thiopyridazine, 1 mmol of $NaBH_4$ and 2 mL of toluene, the reactions were carried out at 180°C and 200 °C, respectively (Figure 2.1). Nevertheless, the conversion ranged between 60% - 70% and the results were hard to reproduce. This might be due to a combination of low concentration and the fact, that the reaction could not be carried out under inert atmosphere.

Influence of the thiopyridazine concentration

In order to evaluate the influence of the concentration on the conversion, a series of experiments were performed. Using 3 equiv of thiopyridazine and 4 mmol of $NaBH_4$, the thiopyridazine concentration was set by varying the volume of toluene.

Table 2.3.: different PnH concentrations.

Entry.	c [mol/L]	V [mL]	conv.
1	0.4	10	40%
2	0.7	6	40%
3	1.3	3	75%
4	2.0	2	100%

Table 2.4.: different scales.

Entry.	$NaBH_4$ [mmol]	c [mol/L]	conv.
1	8	0.4	2%
2	1	0.5	45%
3	4	0.4	40%
4	4	2.0	100%

Table 2.3 lists the conversions, obtained with different PnH concentrations, ranging from 0.4 M to 2.0 M. With increasing concentration of thiopyridazine, the yield increases steadily until full conversion can be obtained with a 2.0 M thiopyridazine solution. Varying the scale of the reaction (Table 2.4), does not lead to the same conversions. Doubling the scale to 8 mmol of $NaBH_4$ in a 0.4 M PnH solution yields only 2% conversion. Decreasing the scale to 1 mmol of $NaBH_4$ in a 0.5 M PnH solution gives a slightly better conversion than using 4 mmol of $NaBH_4$ in a 0.4 M PnH solution. Comparing entries 2-4 in table 2.4 and entries 1-4 in table 2.3 suggests, that a scale of 1 mmol $NaBH_4$ in a 2.0 M PnH solution might yield good conversions as well.

2.1.2. Work up and purification

In order to purify the scorpionate ligand, the optimal conditions and methods for the work up were investigated. For this purpose, the product mixture of the reaction described in table 2.1, entry 3 was chosen as it contains an additional equiv of PnH. A modified work up compared to the published potassium salt was applied, where the crude product was triturated in pentane and the resulting precipitate was filtered and dried in vacuo to obtain the product in high yield. With an equimolar mixture of product and starting material, different purification methods were tested.

Table 2.5.: different purification methods.

method	solvent	purity
Wash	hot pentane	54%
Wash	hot cyclohexane	82%
Soxhlet	pentane	>95%
Soxhlet	cyclohexane	>97%

Table 2.5 summarizes the different purification methods and the resulting purities. It shows, that the purification via soxhlet extraction leads to the best results. While the scorpionate ligand is not soluble in cyclohexane or pentane, the thiopyridazine is only slightly soluble in these solvents, so that simple washing only removes it partially. Using a reversed soxhlet extraction for purification, the insoluble scorpionate is collected in the extraction chamber and over a period of 12 h (overnight), the impurities are slowly dissolved and enriched in the soxhlet flask. The resulting solid can be removed from the extraction chamber and dried in vacuo, to obtain the product in high yields. NMR and IR spectroscopy showed the product to be highly pure. Additionally, the extracted thiopyridazine can be recycled by evaporation and recrystallization from ethanol to be re-used.

2.1.3. Decomposition of the scorpionate ligand

Repeated NMR measurements of a sample of Na[Tn^{tBu}] in different solvents revealed rapid decomposition of the ligand. Figure 2.2 shows the stacked ^{1}H NMR spectra of the sample in methanol. After 0.5 hours, the signal for the tBu group of the scorpionate ligand at 1.05 ppm is predominant. With increasing time, it decreases steadily and the signals for the tBu group of **PnH** at 1.32 ppm increases. Furthermore a third peak appears at 1.18 ppm, that can be assigned to the tBu group of the Pn-disulfide (**Pn$_2$**). The increase of the aromatic **PnH** peaks can also be seen at 7.47 ppm (the second doublet is overlapped by the scorpionate ligand).

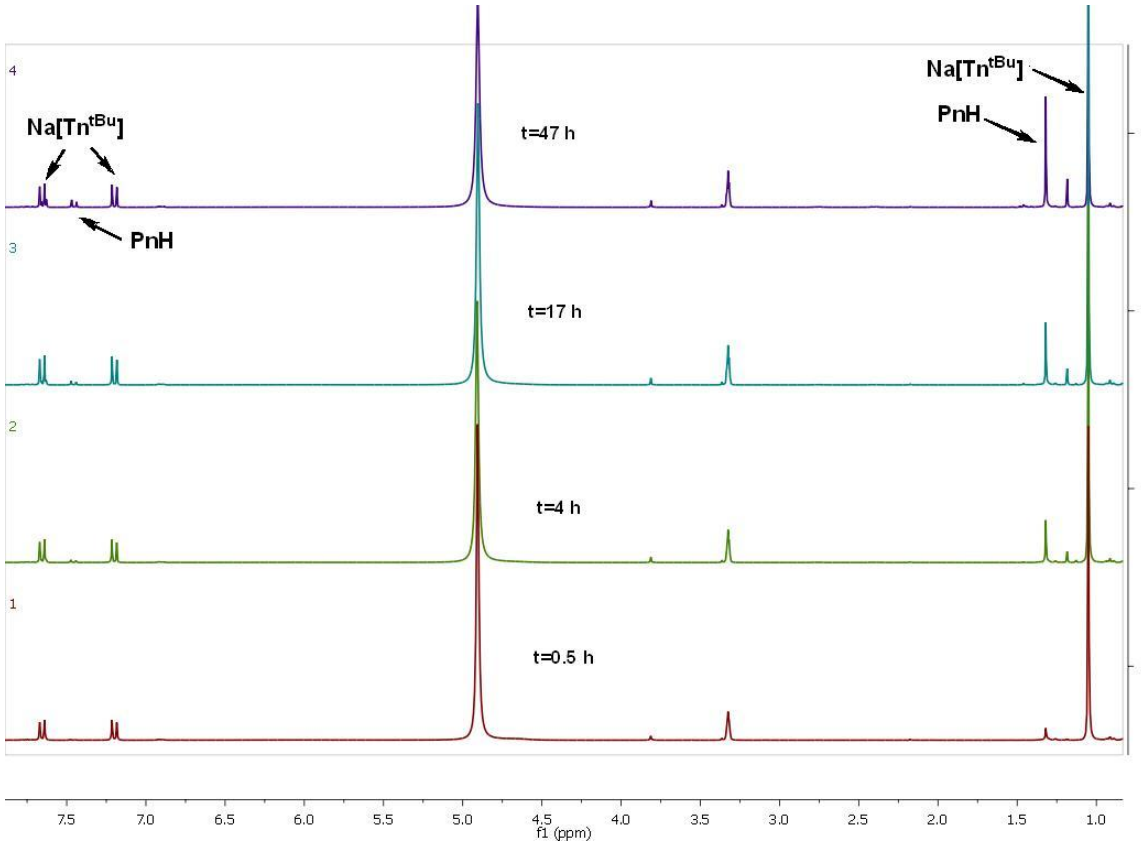

Figure 2.2.: stacked ^{1}H NMR spectra of **1** in methanol over a period of time.

The ratio of the integral of the tBu signal of the scorpionate ligand at 1.05 ppm and the integrals of the signals for the tBu groups of **PnH** and **Pn$_2$** at 1.32 ppm and 1.18 ppm, respectively, gives the concentration of Na[Tn^{tBu}] in the mixture. Figure 2.3 shows the plotting of the Na[Tn^{tBu}] concentration against time in different NMR-solvents.

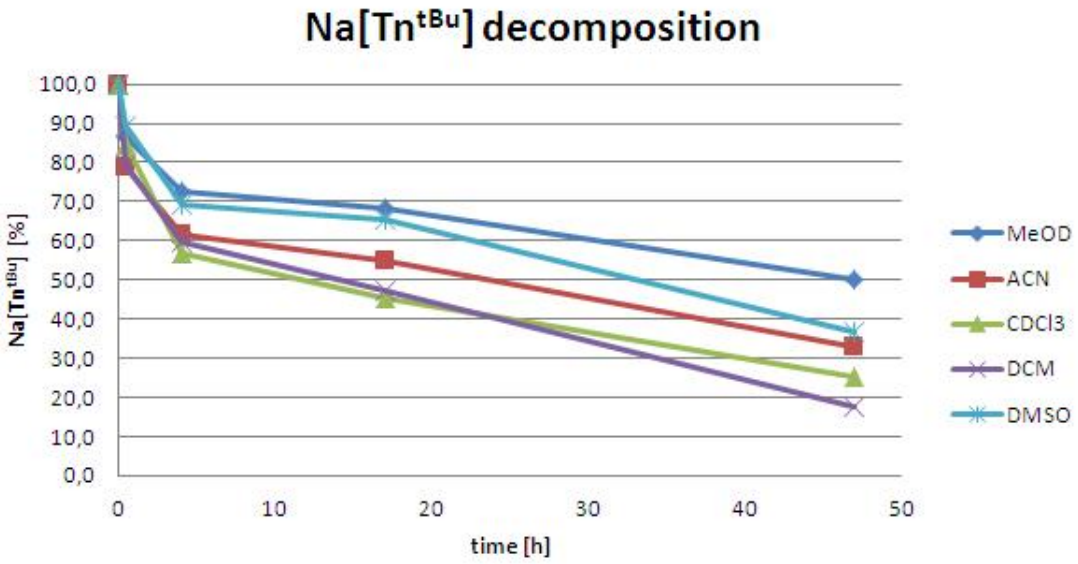

Figure 2.3.: decomposition of the scorpionate in different solvents.

Clearly, the scorpionate ligand decomposes rapidly in all tested solvents. After 47 hours in methanol, only 50% of the compound is left. Changing the solvent to deuterated chloroform or deuterated dichloromethane, 75% and 80% of the ligand is decomposed, respectively. Bearing in mind, that the B-N bond of the scorpionate is the most fragile bond in the molecule, hydrolysis may be the cause of the decomposition. However, comparing the decomposition rate of the scorpionate in methanol, which contains the highest amount of water, the rate is the lowest. This indicates, that hydrolysis is probably not the only cause of the decomposition.

The decomposition under inert atmosphere was also investigated. Therefore, the samples were prepared and dissolved under nitrogen atmosphere and stored in air-tight NMR tubes.

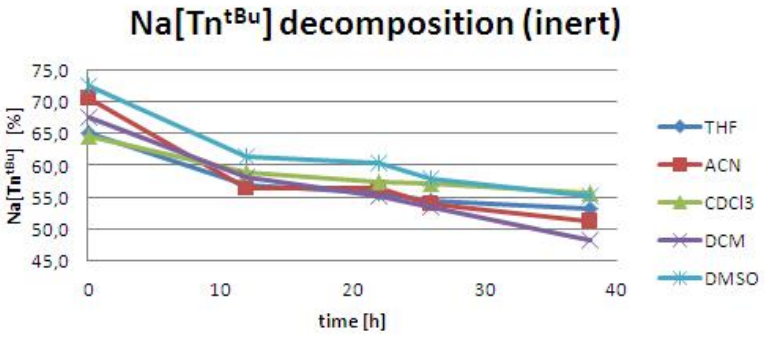

Figure 2.4.: decomposition of the scorpionate under inert atmosphere.

Figure 2.4 shows the decomposition of the scorpionate ligand under inert atmosphere. The scorpionate concentration was calculated analogous to the concentration in figure 2.3 and was plotted against the time. Under inert atmosphere, the compound decomposes in all solvents and after 38 hours, only 55%-48% of Na[Tn^{tBu}] are left, therefore excluding oxygen as the cause of degradation.

Compared to the decomposition in air, under inert atmosphere, the decomposition rate is slower. Furthermore, the decomposition is almost independent of the solvent and decomposes with the same rate.

Additionally, the decomposition was followed by UV-Vis spectroscopy. A 0.1 mM solution of **PnH** and Na[Tn^{tBu}] in methanol was measured over a period of time. The resulting thiopyridazine spectra did not change over time, however, the spectra of the scorpionate ligand changed.

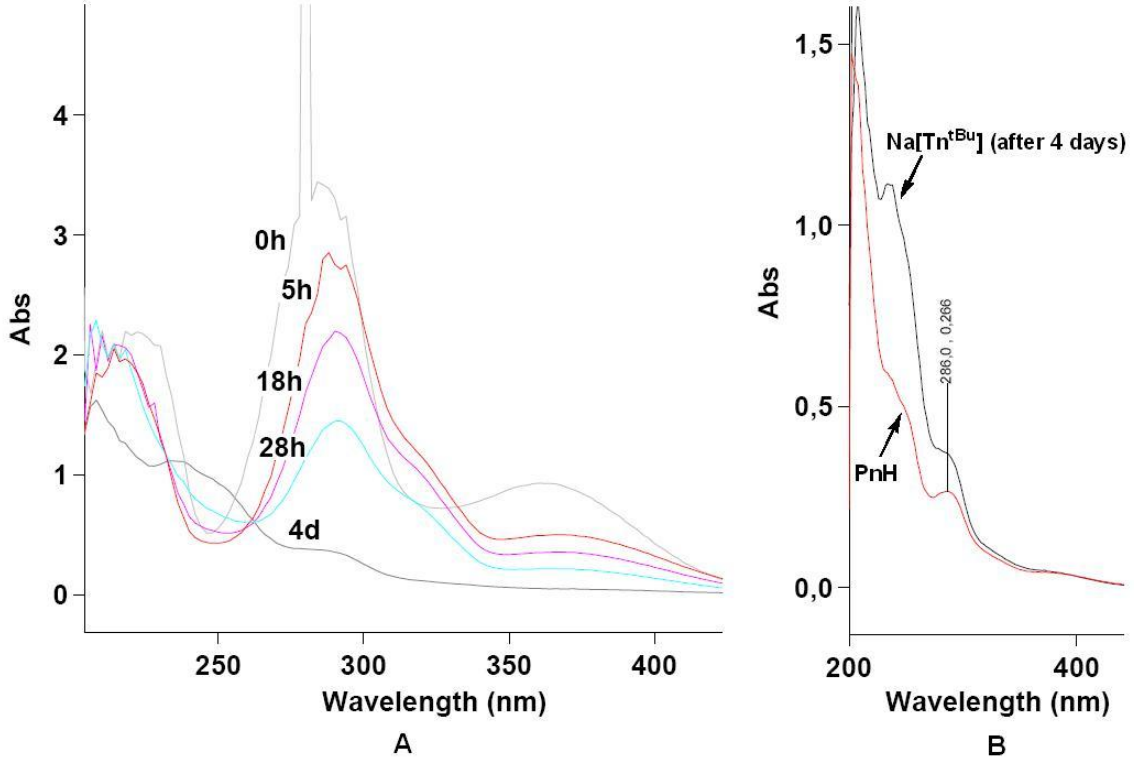

Figure 2.5.: A: UV-Vis spectra of Na[Tn^{tBu}] over time. B: overlay of Na[Tn^{tBu}] after 4 days and **PnH**.

The change of the UV-spectra of Na[Tn^{tBu}] over time is illustrated in figure 2.5A. The absorption maxima at 283 nm and 360 nm decreases rapidly and shifts to 285 nm and 370 nm, respectively. Figure 2.5B shows the overlay of the scorpionate spectrum after 4 days and the **PnH** spectrum. The common absorption maximum of the two spectra at 285 nm is highlighted. These results indicate, that with increasing time, the scorpionate ligand decomposes and its UV-Vis spectra assimilates to the thiopyridazine spectrum. Thus, these results are coherent with the results of the NMR - measurements.
UV-Vis spectra of the scorpionate ligand in methanol were also continuously recorded over a period of 16 hours, under exclusion of light. A control sample, that was exposed to light, was measured before and after the experiment. The obtained spectra are given in figure 2.6.

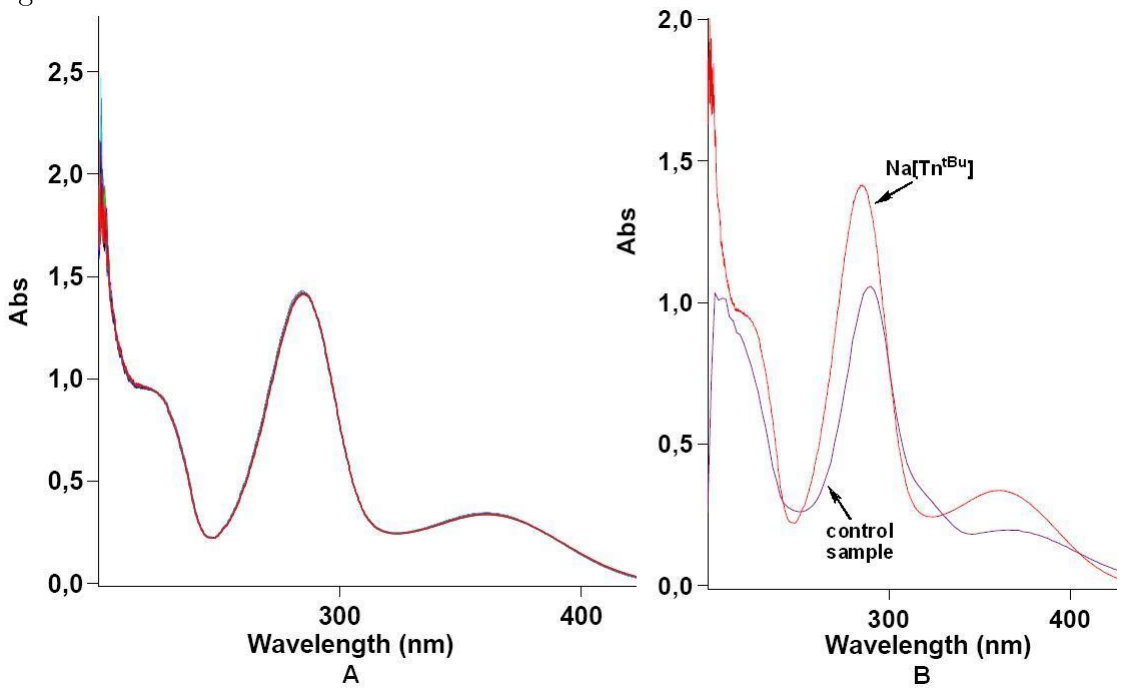

Figure 2.6.: A: UV-Vis spectra of Na[Tn^{tBu}] under light exclusion. B: overlay of Na[Tn^{tBu}] after 16h under light exclusion and the control sample.

Over a period of 16 hours, 19 spectra of the scorpionate ligand were recorded under light exclusion. Figure 2.6A clearly shows, that the spectra do not change over time. The spectrum of the control sample, that was exposed to light, however, shows a decrease of the absorption and a shift to higher wavelengths (Figure 2.6B). These results prove,

that the scorpionate ligand is stable under light exclusion, but decomposes under light exposure.

The sensitivity of the ligand towards light was investigated by irradiation with UV light, using a UV-reactor. A methanolic solution of the pure ligand was placed in a UV-reactor and continuously exposed to UV-irradiation. Samples of 1 mL were taken after 5, 15, 35, 65 and 125 minutes. The methanol was evaporated under light exclusion and the crude sample mixtures were dissolved in deuterated chloroform. The obtained ^{1}H NMR spectra are given in figure 2.7.

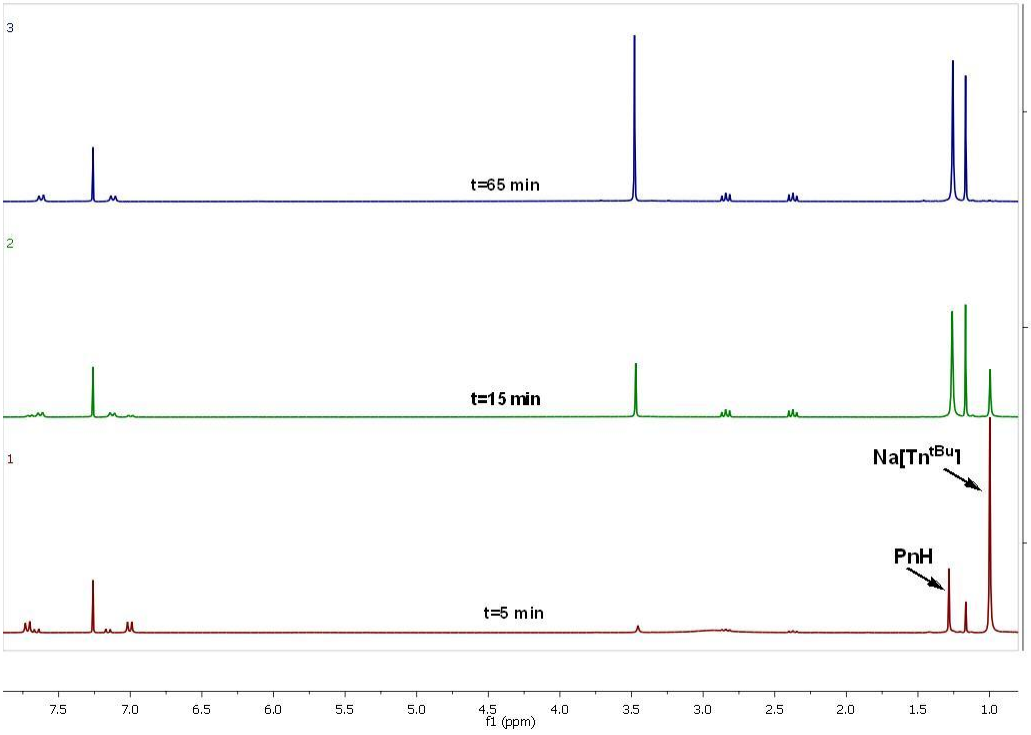

Figure 2.7.: stacked ^{1}H NMR spectra of the UV-induced decomposition of Na[Tn^{tBu}].

After 5 minutes, a signal at 1.28 ppm, representing the tBu group of the **PnH**, can be seen. The signal for the tBu group of the scorpionate ligand at 1.00 ppm decreases rapidly with increasing time and after 65 minutes it is disappeared in the background. The increase of the signals for the **PnH** molecule and the decrease of signals for the Na[Tn^{tBu}] can also be observed in the aromatic region of the spectrum. Furthermore, a singlet at 1.17 ppm

and two triplets at 2.37 ppm and 2.84 ppm appear, integrating in a ratio of 2:2:9.
The sample after 125 minutes was hydrolysed, extracted into CH_2Cl_2 and measured via GC-MS. The spectrum revealed two peaks with masses of 170 g/mol and 168 g/mol, in a ratio of 1:2, respectively. The mass of 170 g/mol and the 3 ^{1}H-NMR signals at 1.17 ppm, 2.37 ppm and 2.84 ppm indicate the formation of a reduced thiopyridazine species, shown in figure 2.8.

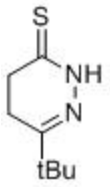

Figure 2.8.: structure of the reduced PnH species.

This structure would fit with the obtained mass of 170 g/mol and with the obtained signals of the ^{1}H NMR spectra. The signals at 2.37 ppm and 2.84 ppm would refer to the 2 protons of the reduced heterocycle and the singlet at 1.17 ppm would fit with the tBu group. Furthermore the ratio of 2:2:9 is identical with this structure.

Another fact, that points towards the reduced PnH species is its ratio to PnH. The 1:2 ratio goes with the decomposition of one molecule of scorpionate ligand. However, the structure of the remaining boron species could not be determined yet.

The concentration of scorpionate ligand in the mixture was calculated analogous to figure 2.3. The graphs for the scorpionate concentration and the logarithm of the scorpionate concentration plotted against the time are given in figure 2.9.

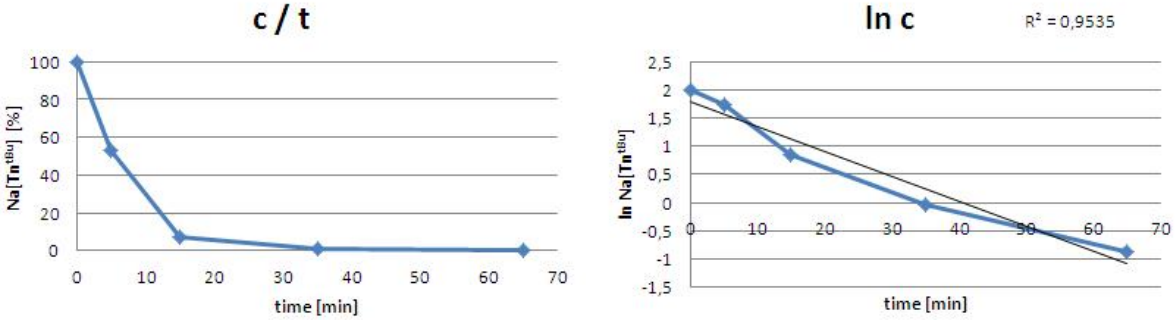

Figure 2.9.: graphical plot of c/t and ln c.

The c/t graph clearly shows the rapid decomposition of the scorpionate ligand under UV-irradiation. After 5 minutes, 45% of the ligand is already decomposed and after 35

minutes, only 7% of the ligand is left. This is significantly faster, than the decomposition under normal light exposure (Figure 2.3), implying, that the ligand is rather UV-light sensitive, than to light of higher wavelengths. The linear relationship of the logarithm of the scorpionate concentration vs the time implies a 1^{st} order kinetic with a linear regression of 95%. However, in order to confirm this, an extended kinetic measurement is required, to exclude other reaction orders.

2.2. Preparation of Tl[Tn^{tBu}] (2)

In order to synthesise metal-scorpionate complexes, the use of a thallium - derived scorpionate species has some significant advantages. In the case of metal halide scorpionate complexes, insoluble Tl-halide side products are formed and can be removed easily. Furthermore, for the synthesis of zinc alkyl complexes, the use of a thallium salt provides a good starting material.[110]

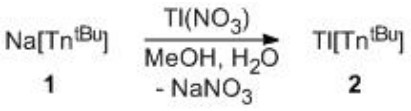

(2.2)

The thallium salt of the scorpionate ligand Tl[Tn^{tBu}] (**2**) was prepared according to eq. 2.2. For the synthesis of **2**, a mixture of methanol/water was used, whereas without water, no conversion was observed. Thus, after addition of an aqueous solution of Tl(NO_3) to a methanolic Na[Tn^{tBu}] solution, a yellow precipitate formed, which can be filtered and dried in vacuo, to obtain the product in good yields (90%). The ^{1}H NMR spectrum of the compound shows one set of signals at 1.03 ppm, 7.06 ppm and 7.76 ppm, respectively. The signal of the B-H proton is not observable in $CDCl_3$. A high-resolution mass spectrometry yielded the M^+ peak with a mass of 718.1880 g/mol, which fits to the calculated Tl[Tn^{tBu}] mass. Single crystals, suitable for X-ray diffraction could be obtained from slow evaporation of a methanolic solution.

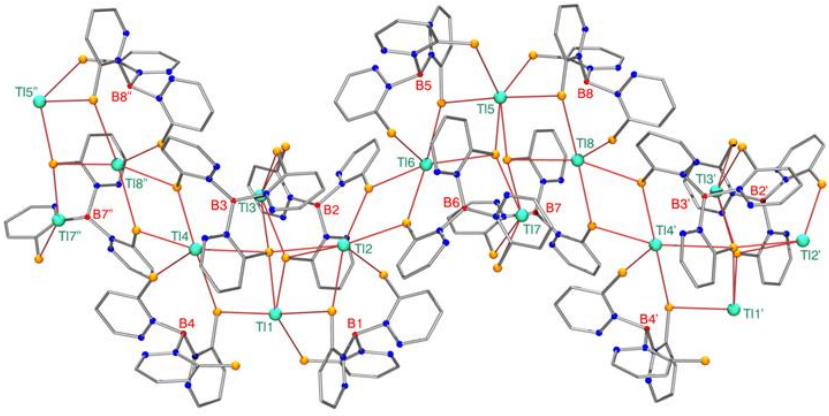

Figure 2.10.: molecular view of compound **2**; crystal structure with 10% probability.[111]

The crystal structure, given in figure 2.10, reveals a polymeric structure, where the unit cell consists of 8 Tl atoms, coordinated by 8 scorpionate ligands. Compared to the K[Tn^{Me}] structure (Figure 1.23), where the K is coordinated by S,N and H_2O, the thallium atoms are only coordinated by sulfur atoms.

Taking a closer look at this complex crystal structure, a new coordination mode is seen. In figure 2.11, the structure is shown in a molecular view, revealing an octahedral coordination of the thallium atoms. Furthermore, it is clearly visible, that one scorpionate coordinates two thallium atoms: while two sulfur atoms coordinate on the same thallium, the third sulfur atom bridges to a second thallium atom.

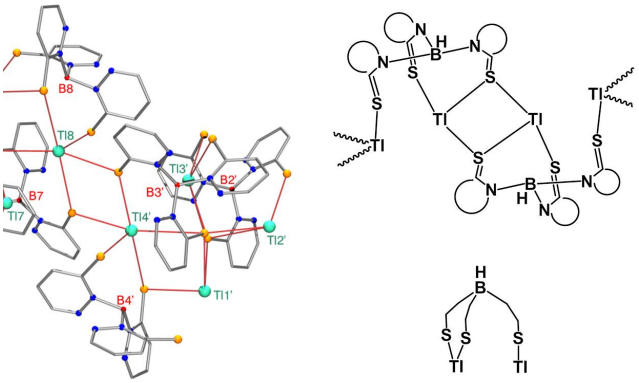

Figure 2.11.: detailed view of the Tl[Tn^{tBu}] crystal structure.

Therefore, the structure can be simplified to a $\kappa - S, S, Tl^1, \kappa - S, Tl^2$ coordination. A similar coordination mode, where one sulfur is bridging two thallium atoms has already been published by Gardinier, using a thallium salt of the tris (mercaptothiadiazolyl) borate ligand.[110]

2.3. Synthesis of a scorpionate zinc-alkyl complex

The thallium salt **2** was used as a starting material for the preparation of zinc alkyl complexes, according to eq. 2.3. The preparation of organometallic zinc scorpionate complexes has previously been described by Kumar et al., using triazole - based scorpionate ligands.[52]

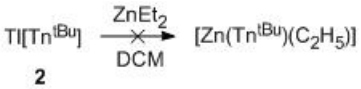

(2.3)

Under inert atmosphere, diethyl zinc was slowly added to a stirred solution of **2** in DCM

and was stirred overnight at room temperature. The resulting dark brown suspension was centrifugated and the brown solution was decanted and evaporated to give an orange powder. Subsequent NMR analysis of the compound revealed full decomposition of the ligand. Single crystals of the decomposition product could be obtained from slow evaporation of a THF solution. The obtained crystal structure is shown in figure 2.12.

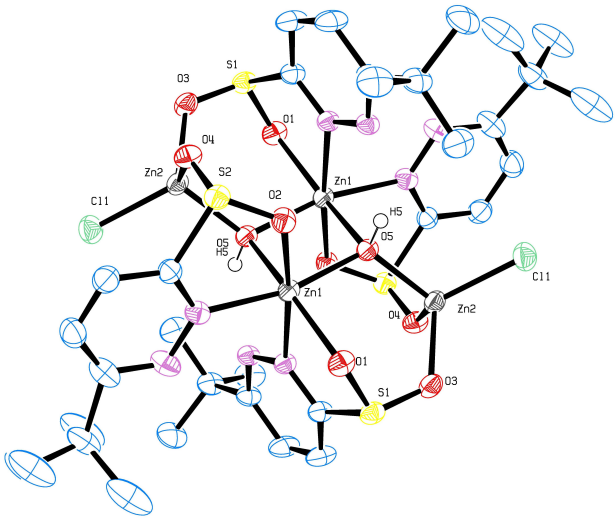

Figure 2.12.: molecular view of the [Zn(Tn^{tBu}(Et)] decomposition product.

The X-ray diffraction analysis revealed a zinc compound in which the scorpionate ligand is no longer intact. However, the thiopyridazine moieties remained in the structure. Furthermore, the thio groups are oxidised.

The structure consists of two octahedrally coordinated- and two tetrahedrally coordinated zinc atoms and four oxidised thiopyridazines. The four zinc atoms are connected to each other via a μ_3-OH (O5).

The oxidised sulfinato-pyridazines bridge the two differently coordinated zinc atoms via their oxygen and nitrogen donors and the tetrahedrally coordinated zinc atoms bear a chlorine atom, which might origin from the used dichloromethane.

Because of the fact, that only single crystals could be obtained, no other data on this structure are available. Nevertheless, this not-reproducible structure gives a good hint of what can happen applying the thallium salt to zinc alkyl species.

2.4. Synthesis of zinc-halide complexes coordinated by $[Tn^{tBu}]^-$

Zinc halide complexes with scorpionate ligands are a useful precursor for the preparation of zinc hydroxide or zinc alkyl complexes because they can be substituted easily. Furthermore, the synthesis of zinc halide complexes is simple and the resulting insoluble metal halide side product can be easily removed.
Starting with the sodium salt of the scorpionate ligand (**1**), several zinc halide complexes could be isolated. Depending on the solvent, different products were obtained.

2.4.1. Synthesis of $[ZnBr(Tn^{tBu})(THF)]$ (3)

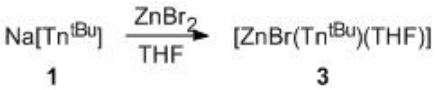

(2.4)

Addition of zinc bromine to a solution of $Na[Tn^{tBu}]$ in THF leads to the formation of $[ZnBr(Tn^{tBu})(THF)]$ (**3a**), according to eq. 2.4. Under inert atmosphere and light exclusion, a yellow powder could be isolated in 70% yield. The ^{1}H NMR spectrum of the product revealed 3 sets of signals for the pyridazines, that are consistent with an asymmetric coordination of $[Tn^{tBu}]$. The ^{1}H NMR spectra of the aromatic signals of the starting material and the product are stacked in figure 2.13.

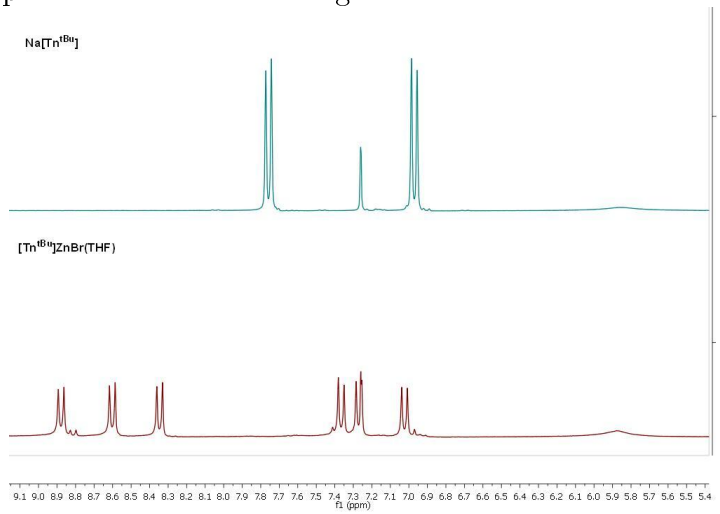

Figure 2.13.: stacking of the ^{1}H-NMR spectra of starting material and product.

It is clearly seen, that in the starting material, the aromatic protons give 2 signals. In the zinc-scorpionate complex **3a**, however, the signals split up and each proton gives an individual resonance. This indicates a loss of symmetry, where each "thiopyridazine - arm" has a different chemical environment. Furthermore, resonances assignable to one equivalent of a coordinated THF molecule are found in the spectrum at 1.89 ppm and 3.84 ppm. This can also be observed in the ^{13}C-NMR spectrum.

Upon standing under inert atmosphere, a yellow solution of complex **3a** in $CDCl_3$ turned deep blue. A subsequent NMR analysis of this blue solution revealed 3 sets of signals, however the resonances for uncoordinated THF molecules can be observed. Additionally, the aromatic signals in the ^{1}H NMR spectrum of **3b** are significantly shifted, compared to complex **3a** (Figure 2.14).

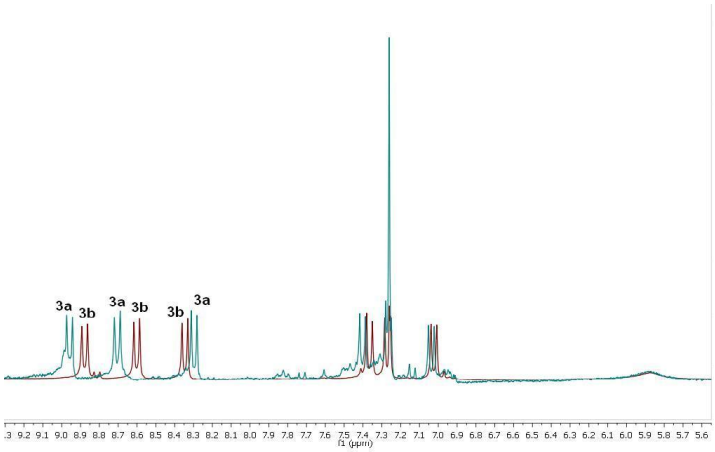

Figure 2.14.: superimposed ^{1}H-NMR spectra of **3a** and **3b**.

While the signals of one proton of the thiopyridazine moiety (3 signals) are significantly shifted towards lower fields, the other 3 proton signals and the broad singlet for the B-H resonance do not change. Single crystals of the moisture - sensitive, blue complex **3b** could be obtained from slow diffusion of pentane into a $CDCl_3$ solution. They proved to be difficult to handle due to fast solvent evaporation, hampering the quality of the crystals and thus the obtained data. Although for the discussion of bond lengths and angles, the accuracy is not large enough, it showed the connectivity. Figure 2.15 shows the molecular view from the top. In this hexameric structure, 6 zinc-bromine moieties and 6 scorpionate ligands can be found. Furthermore, the structure shows an interesting form, where the sulfur atoms are arranged in a cylindrical shape, providing an inner core

and the tBu groups forming an outer sphere. Additionally, the crystal structure shows pentane molecules surrounding the outer sphere.

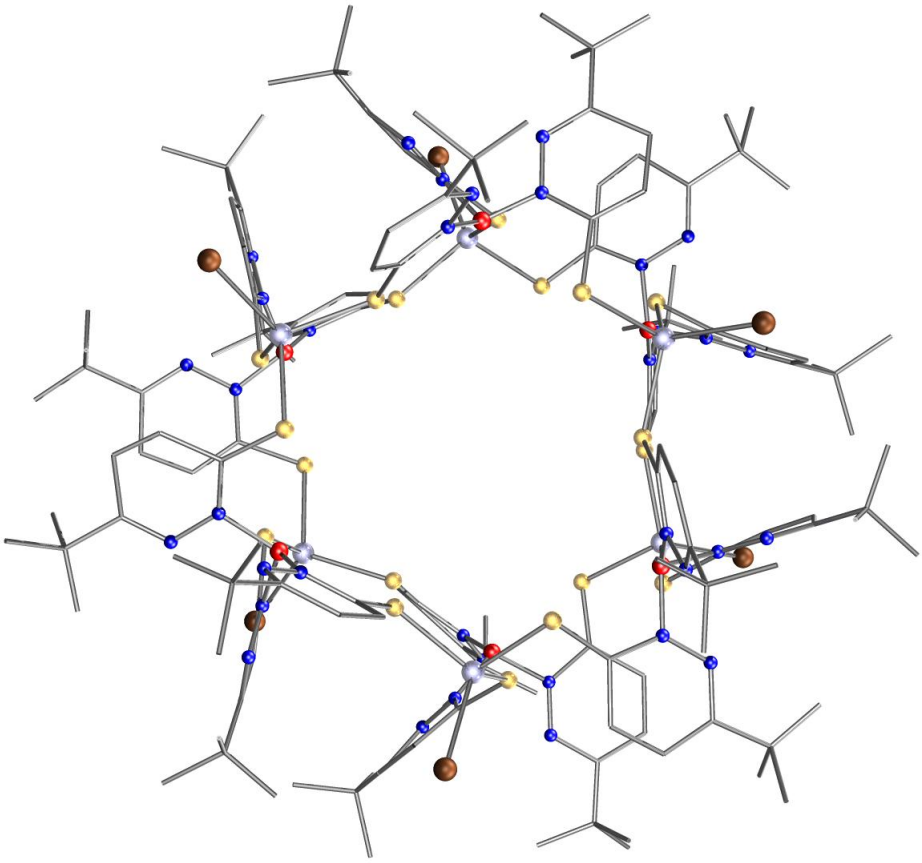

Figure 2.15.: molecular view of the crystal structure of complex **3b**; pentane molecules and H atoms omitted for clarity.

The complicated structure can be simplified by removing all atoms except the zinc, bromine and boron atoms. Figure 2.16 shows the resulting frame and the coordination motive of the scorpionate ligand in the crystal structure.

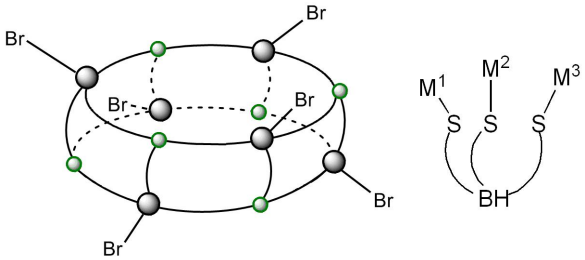

Figure 2.16.: frame of the [ZnBr(Tn^{tBu})] crystal structure and monodentate coordination mode of the scorpionate ligand.

The circular arrangement of alternating zinc and boron atoms leads to three bromine atoms alternating pointing up- and down, respectively. Furthermore, the zinc atoms are tetrahedrally coordinated by different "arms" of the scorpionates central boron atom, providing a new coordination motive of a monodentate scorpionate ligand.

2.4.2. Synthesis of [ZnI(Tn^{tBu})(THF)] (4)

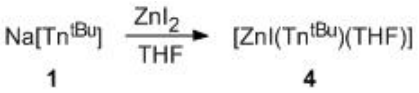

(2.5)

In analogy to compound **3a**, the zinc-iodine complex **4** was prepared according to eq. 2.5. Under inert atmosphere and under light exclusion, the compound could be isolated as a yellow powder in 68% yield. The compound proved to be air - and moisture stable and an IR-measurement revealed a B-H resonance at 2565 cm^{-1}. The ^{1}H NMR spectrum of complex **4** revealed a significant difference to the zinc bromine complex **3a**.

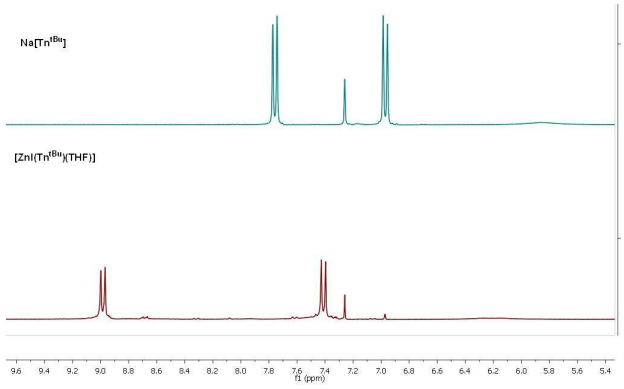

Figure 2.17.: stacking of the aromatic region of the ^{1}H-NMR spectra of Na[Tn^{tBu}] and complex **4**.

As expected, the aromatic signals of complex **4** (Figure 2.17) are shifted towards lower field, and the resonances for one molecule of coordinating THF can be found. But instead of an asymmetric complex like in complex **3a**, only one set of signals is observed, indicating a symmetric complex. This symmetry can also be seen in the ^{13}C - NMR spectrum.

Another difference to the zinc-bromine complex **3a** is the fact, that no coloured hexameric complex is formed upon standing. After 1 month under inert atmosphere, neither the colour of the solution, nor the NMR - spectra changes. This suggests, that the THF is more tightly bound to the zinc-iodine complex than to the corresponding bromine species.

The increased down-fielded shift of the resonances for the coordinated molecule of THF in the [ZnI(Tn^{tBu})(THF)] complex strengthens the hypothesis of a stronger coordinating solvent.
Despite of the differences between the zinc bromine and iodine species, both THF-complexes are air stable and their IR - spectra are identical. These identical spectra can be explained, because their difference - the zinc-halide bond - is beyond the measurement range of the used IR-spectrometer.[112]

2.4.3. Synthesis of [ZnI(Tn^{tBu})] (5)

The preparation of a compound similar to **3b**, albeit with iodine instead of bromine attached to the zinc was attempted. Under inert atmosphere, ZnI_2 was added to a solution of Na[Tn^{tBu}] in dry DCM and stirred overnight under light exclusion. The resulting beige solution was evaporated to yield [ZnI(Tn^{tBu})] (**5**) as a light green powder in 62% yield. The complex is air- and moisture sensitive and the ^{1}H NMR spectrum shows 3 sets of signals, that are identical to the ^{1}H NMR spectrum of complex **3b**. These identical spectra give rise to the assumption, that in solution, the zinc-bromine and the zinc-iodine complex provide the same species, whereas upon crystallization, different solid species are formed. One explanation of this ambivalence would imply a cationic complex, that is formed in solution. However, these ambiguous results are a topic of further investigation, to understand the coordination geometry in the two complexes.

Re-dissolving complex **5** in THF leads to a yellow solution, that yielded a yellow, air-stable powder after evaporation. A subsequent NMR analysis of the obtained compound showed 3 sets of signals and resonances that indicate one molecule of a coordinated THF. These results imply, that the symmetric, THF-coordinated zinc iodine complex **4** can not be obtained by a simple re-coordination of THF.

2.4.4. Comparison of compounds 2-5 to other [Tn]-metal complexes

Comparing these [Tn^{tBu}]-coordinated zinc complexes with previously published copper, nickel and cobalt based scorpionate complexes, a difference can be observed. In copper complexes, the scorpionate ligand coordinates in a bi- and tridentate manner, providing a copper-hydride interaction.[108] Coordinating the ligand to nickel or cobalt, the corresponding boratrane complexes are formed.[106] In contrast to these metals, zinc provides a completely different coordination behaviour. Without coordinating solvent, the scorpionate ligand coordinates in a monodentate fashion, leading to a coloured hexameric complex. Although the crystallographic data are vague, they show an inverted boron atom, where the hydrogen points towards the metal center. Furthermore, due to the lack of redox-activity, no tridentate boratrane complexes like the nickel and cobalt species could be obtained. Still, the question of the solvent-coordinated structures **3** and **4** have to be answered, to fully compare the zinc-complexes with other [Tn^{tBu}]-based complexes.

2.5. Synthesis of a zinc-halide complex coordinated by [^{Pn}Bm]$^-$ (6)

The coordination behaviour of the electron deficient thiopyridazine based scorpionate ligand was compared to electron rich scorpionate ligands. Therefore, a previously published mixed hybrid scorpionate ligand, based on two thiomethimidazoles and one thiopyridazine was used.[109]

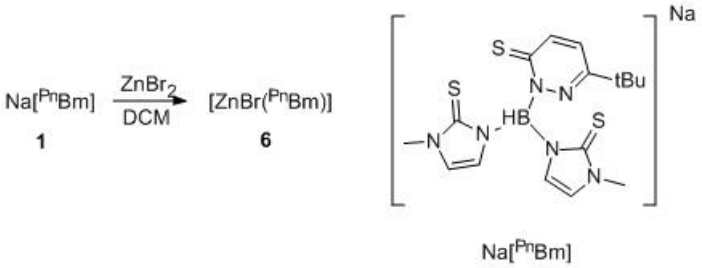

(2.6)

According to eq. 2.6 the moisture and air stable Na[^{Pn}Bm] ligand was dissolved in DCM, anhydrous zinc bromine was added and the beige solution was stirred overnight. The resulting beige suspension was filtered and dried in vacuo to obtain [^{Pn}Bm]ZnBr (**6**) as a white powder in 82% yield. The complex is air and moisture stable and does not decompose upon heating to 60°C. The ^{1}H NMR spectrum shows a singlet at 1.13 ppm, another singlet at 3.50 ppm, a broad singlet at 5.29 ppm and 4 doublets in the aromatic region at 6.79 ppm, 7.24 ppm, 7.33 ppm and 7.57 ppm, respectively. While the singlets in the aliphatic region refer to the tBu group of the thiopyridazine and the two Me groups of the methimidazole moiety, the broad singlet at 5.29 ppm refers to the B-H resonance. The fact, that only one set of signals is obtained points towards a symmetric complex. Single crystals, suitable for X-ray diffraction analysis could be obtained from layering a DCM solution of **6** with cyclohexane. A molecular view is given in figure 2.18 and selected bond lengths and angles are listed in table 2.6.

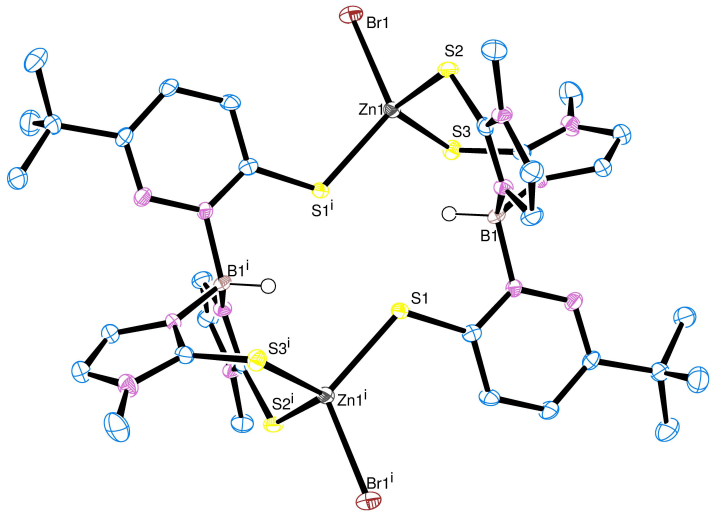

Figure 2.18.: crystal structure of complex **6**, hydrogen atoms omitted for clarity, except the H atom at boron.

Table 2.6.: selected bond lengths and angles for complex **6**.

bond lengths [Å]		bond angles [°]	
Zn1 - S1	2.3582(11)	Br1 - Zn1 - S1	116.21(3)
Zn1 - S2	2.3613(12)	Br1 - Zn1 - S2	98.32(3)
Zn1 - S3	2.3604(12)	Br1 - Zn1 - S3	107.31(3)
Zn1 - Br1	2.4090(6)	Br1 - Zn1 - H1	174.86(4)

The structure consists of two tetrahedrally coordinated zinc atoms, that are bridged via the thiopyridazine of the scorpionate. Interestingly, the boron atoms are involved in B-H-Zn interaction, leading to a Zn-B distance of 3.379(8) Å. This beginning interaction is supported by the elongated zinc bromine bond from 2.22 Å in $ZnBr_2$ to 2.4090(6) Å.[113] Additionally, the scorpionate ligand does not coordinate tridentate but bidentate, using the third donor to bridge the two monomeric units. The reduced coordination capacity of the thiopyridazine moiety is consistent with its electron deficiency. The bidentate coordinating donors both belong to the electron rich thio-methimidazole, while the electron deficient thiopyridazine is used for the bridging. However, comparing the bond lengths of the zinc - sulfur bonds, they all show almost the same bond length of 2.3599(78) Å. This shows, that there is negligible difference in the Zn-S bond strengths, whether the

sulfur derives from an electron rich 5-membered ring or an electron deficient 6-membered heterocycle.

The dimeric structure shows high similarity to a Cu(I) complex, with the same ligand precursor described by the Mösch-Zanetti group, where also a copper-dimer was obtained.[109] In the Cu complex, the thiopyridazine arm also bridges the two Cu - centers, but they clearly observed a copper - hydride interaction with a Cu-B distance of 2.798(9) Å. This is significantly closer than the Zn-B distance in complex **6**, where only the enlarged Zn-Br bond indicates a B-H-Zn interaction.

Comparing the hybrid [ZnBr(^{Pn}Bm)] scorpionate complex with the [Tn^{tBu}]Zn-halide complexes, a significant difference in the coordination mode can be stated. While the homoscorpionate coordinates only in a monodentate fashion, resulting in a hexameric structure, the mixed hybrid-scorpionate, however, coordinates bidentate, forming a thermally stable dimer.

2.6. Synthesis of Fe(II) complexes

The coordination mode of the thiopyridazine based scorpionate ligand in zinc chemistry was compared to its coordination behaviour in iron complexes. Therefore, the sodium salt of the scorpionate (**1**) and the free thiopyridazine (**PnH**) were reacted with iron(II)triflate ($Fe(OTf)_2$) to obtain iron(II) complexes with the corresponding ligands.

2.6.1. Synthesis of [Fe(Tn^{tBu})(OTf)] (7)

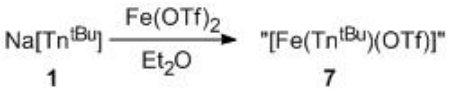

(2.7)

According to eq. 2.7, Na[Tn^{tBu}] was stirred together with $Fe(OTf)_2$ in dry diethyl ether. After 12 hours, the orange suspension was filtrated and dried in vacuo to obtain the product as a light red, micro crystalline solid. An IR analysis of the air stable complex showed a B-H resonance at 2455 cm^{-1} and a high-resolution mass spectrometry reveals a mass of 1287.238 g/mol, which fits to the calculated mass of a dimeric structure of the formula $[L_2Fe_2(OTf)]^+$. Based on the putative formula [Fe(Tn^{tBu})(OTf)], the reaction yielded 94%. Due to the paramagnetic properties of the sample, a NMR analysis showed no resonances. Single crystals could be obtained from a toluene solution, however, the obtained crystals were too small for X-ray diffraction.

Comparing the IR spectrum of the complex, a significant shift of the BH - peak from 2536 cm^{-1} in the ligand to 2455 cm^{-1} in the complex is observed. Compared to the BH-shifts in the corresponding zinc-halide complexes (2562 cm^{-1} and 2565 cm^{-1}, respectively), the high shift to lower wave numbers implies a significantly looser bound boron hydride.

2.6.2. Synthesis of a $[Fe(PnS_3Pn)_2](OTf)_2$ complex (8)

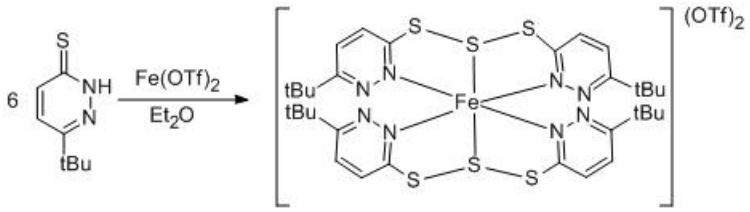

(2.8)

The attempt to prepare a thiopyridazine coordinated Fe-complex led to the formation of complex **8**, according to eq. 2.8. Stirring 6 equivalents of **PnH** and 1 equiv. of $Fe(OTf)_2$ under inert atmosphere in dry diethyl ether for 16 hours, an orange suspension forms. The precipitate is filtered and dried in vacuo to obtain $Fe[(PnS_3Pn)_2](OTf)_2$ (**8**) as an orange solid in 85% yield. Due to strong paramagnetic properties, NMR analysis of the complex showed no resonances. Subsequent measurements with a Gouy balance yielded a value for the magnetic susceptibility, that indicates 4 unpaired electrons. Single crystals, suitable for X-ray diffraction, could be obtained from a concentrated DCM solution. The crystal structure of complex **8** is illustrated in figure 2.19 and selected bond lengths and angles are listed in table 2.7.

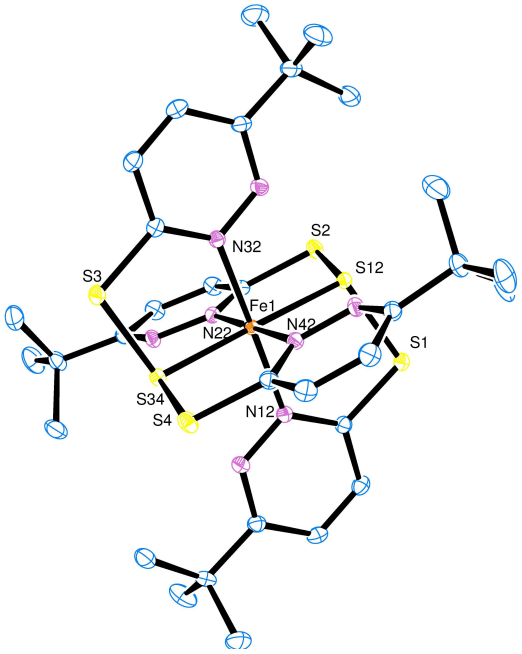

Figure 2.19.: crystal structure of **8**; H-atoms and OTf groups were omitted for clarity.

Table 2.7.: selected bond lengths and angles for complex **8**.

bond lengths [Å]		bond angles [°]	
Fe1 - N22	1.9700(14)	N12 - Fe1 - N32	179.08(6)
Fe1 - N32	1.9701(14)	N22 - Fe1 - N42	179.39(6)
Fe1 - N12	1.9724(14)	S12 - Fe1 - S34	179.111(18)
Fe1 - N42	1.9765(14)	S2 - S12 - S1	103.82(2)
Fe1 - S34	2.2338(4)	S2 - S12 - Fe1	103.01(2)
Fe1 - S12	2.2353(4)	S1 - S12 - Fe1	101.79(2)
S1 - S12	2.0831(6)	S3 - S34 - S4	103.67(2)
S12 - S2	2.0743(6)	S3 - S34 - Fe1	102.63(2)
S3 - S34	2.0780(6)	S4 - S34 - Fe4	102.38(2)
S34 - S4	2.0826(6)		

The octahedral environment of the Fe atom comprises 4 N atoms of the pyridazine rings and of two central S atoms of the S_3 bridges between these rings, providing a $\kappa - N, S, N$ facial coordination. For each iron complex unit, two triflate anions can be found in the structure, consistent with an iron(II) complex. The compound is highly symmetric with the four tBu groups shielding the core against external impacts and therefore is apolar. This might be a reason for the compounds inertness in water or other solvents.
Stirring the orange powder in water for half an hour does not change the sample, as subsequent crystallization and X-ray diffraction shows. Furthermore, reactions with a 3:1 stoichiometry with respect to the iron precursor in dry, coordinating solvents do not lead to a tetrahedrally, solvent coordinated complex, but results in formation of compound **8**.

For this reaction, the origin of the coordinating sulfur is of particular interest. NMR - measurements and elemental analysis of **PnH**, however, showed pure starting material. This implies, that the sulfur derives from a thiopyridazine molecule. Therefore, a ratio of 6:1 with respect to the iron precursor, would lead to the trisulfide - bridged product.
Interestingly, a copper - derived trisulfide bridged complex has already been reported by Delgado and co-workers in 2011.[114] However, they obtained the complex only in traces

(8% yield) starting with a bipyridine disulfide species. The reaction of thiopyridazine with Fe(II), however, is high yielding and the complex can be isolated without further purification.

Chapter 3.

Experimental

3.1. General methods

Chemicals were purchased from commercial sources and used without further purification. Air- and moisture sensitive chemicals, as well as $NaBH_4$ were stored in the glove box, to prevent hydrolysis or decomposition. The starting material, 6- tert- butyl- pyridazine-3-on, **PnH** and Na[^{Pn}Bm] were synthesised according to literature procedures.[106,109] All reactions were - unless stated otherwise - carried out under inert atmosphere using standard Schlenk and glove-box techniques. Solvents were purified via a Pure Solv. Solvent Purification System and their dryness was checked via a Metrohm 831 KF Coulometer. NMR spectra were measured on a Bruker Avance III 300 MHz spectrometer at 25°C. The shifts of the ^{1}H and ^{13}C NMR spectra are given in ppm and referred to residual protons in the solvent. Signals are described as s (singlet), bs (broad singlet), d (doublet), t (triplet) and m (multiplet)and coupling constants are given in Hertz (Hz).

IR spectra were directly measured on a Bruker ALPHA-P Diamant ATR-FTIR spectrometer at a resolution of 2 cm^{-1}. Signal intensities are assigned according to their relative intensities as strong (s), medium (m), weak (w) or very weak (vw). All IR-bands are listed in cm^{-1}. Mass spectra were recorded with an Agilent 5973 MSD − Direct Probe using the EI ionization technique. Elemental analyses were carried out using a Heraeus Vario Elementar automatic analyzer at the Technical University of Graz. Sus-

ceptibility measurements were obtained on a MSB Auto Magnetic Susceptibility Balance of Johnson Matthey Alfa. UV-Vis measurements were carried out with a Varian 50 Conc UV-Vis Spectrophotometer. Photochemical reactions were carried out using an Immersion Well Photochemical Reactor RQ125 with a 125 watt medium pressure mercury lamp 3010/PX0686.

X-ray structure determinations were performed on a Bruker AXS SMART APEX 2 CCD diffractometer by using graphite-monochromated Mo-K_α radiation from a fine-focus sealed tube at 100 K. SHELXS-97 was used as structure solution and structure refinement program.[115] Full-matrix least-squares on F^2 was employed as refinement method. The non-hydrogen atoms were refined with anisotropic displacement parameters without any constraints.

3.2. Ligand Synthesis

3.2.1. Sodium [tris (6- tert- butyl- 3-thiopyridazinyl) borate] Na[Tn^{tBu}] (1)

The sodium salt of the scorpionate ligand was prepared analogous to the published potassium salt, however, instead of KBH_4, $NaBH_4$ was used. In the glove box, 151 mg (1.0 equiv, 4 mmol) of fresh sodium borohydride was combined with 2.0 g (3.0 eq., 12 mmol) of **PnH**. The solids were suspended in 2.5 mL of bench top toluene (dry toluene yields no conversion, see results and discussion). Upon heating under reflux, the yellow suspension turns to an orange solution. Hydrogen starts to evolve at 100°C and after 1h stirring under reflux, a precipitate forms. After 2 days, hydrogen evolution ceased and the reaction mixture was cooled to room temperature and triturated in 100 mL of pentane. Immediately, a yellow precipitate formed and was filtered and dried in vacuo. The crude product was purified via reversed soxhlet extraction overnight in cyclohexane. After drying in vacuo, the product was obtained as a light yellow powder. Yield: 1.83g (85%)

^{1}H NMR (300 MHz, $CDCl_3$) δ (ppm): 7.74 (d, J=9.2Hz, 3H, ArH), 6.99 (d, J=9.2Hz, 3H, ArH), 5.89 (bs, 1H, BH), 0.99 (s, 27H, CH_3).
^{13}C NMR (300 MHz, $CDCl_3$) δ (ppm): 178.80 (Ar-**C**), 160.43(Ar-**C**), 142.00(Ar-**C**), 122.67 (Ar-**C**), 36.33(R-**C**-$(CH_3)_3$), 29.17 (R-C-(**C**$H_3)_3$).

3.2.2. UV-induced decomposition of 1

A methanolic solution consisting of 300 mg (0.56 mmol) of **1** and 75 mL of methanol was prepared. Under light exclusion, the solution was stirred for 5 minutes until all solid was dissolved. The yellow solution was transferred into the nitrogen flushed UV-reactor and subsequently the UV light was turned on. Samples of 1 mL were taken after 5, 15, 35, 65 and 125 minutes, respectively and dried in vacuo. The resulting yellow precipitate was analysed via ^{1}H NMR spectroscopy under light exclusion.

3.2.3. Determination of the decomposition products

After collecting all samples of the UV-induced decomposition of **1**, the remaining solution was evaporated. The yellow precipitate was quenched with 30 mL of water, extracted into 70 mL of DCM, dried over $MgSO_4$ and dried in vacuo to obtain a crude product mixture of the decomposition products. Subsequent GC-MS measurements revealed two signals with M^+ masses of 170 g/mol and 168 g/mol in an approximate relation of 1:2.

3.2.4. Thallium [tris (6- tert- butyl- 3-thiopyridazinyl) borate] (2)

In a 50 mL Erlenmeyer flask, 645 mg (1.0 equiv, 1.2 mmol) **1** were suspended in 10 mL H_2O and 5 mL of methanol. Under stirring, a solution of 620 mg (2.0 eq. 2.4 mmol) thallium nitrate in 10 mL of H_2O was added dropwise. A yellow precipitate forms immediately and after additional 30 minutes of stirring, the solution was filtered and the precipitate was dried in vacuo to obtain pure **2**. Yield: 801 mg (93%).

^{1}H NMR (300 MHz, $CDCl_3$) δ (ppm): 7.76 (d, J=8.9Hz, 3H, ArH), 7.06 (d, J=8.9Hz, 3H, ArH), 1.03 (s, 27H, CH_3).
^{13}C NMR (300 MHz, $CDCl_3$) δ (ppm): 179.08 (Ar-**C**), 161.20 (Ar-**C**), 142.00 (Ar-**C**), 122.46 (Ar-**C**), 36.30 (R-**C**-$(CH_3)_3$), 29.14 (R-C-(**C**$H_3)_3$). M^+ calc.: 718.1846 m/z, found: 718.1880 m/z. Figures of the crystal structure and isotope pattern of the high-resolution mass are given in the appendix.

3.3. Complex Synthesis

3.3.1. [ZnBr(Tn^{tBu})(THF)] (3)

Under inert atmosphere and light exclusion, 200 mg (1.0 equiv, 0.37 mmol) of **1** were mixed with 125 mg (1.5 equiv, 0.56 mmol) of $ZnBr_2$ and dissolved in 5 mL of dry THF. After stirring for 16 h, the beige solution was evaporated to give a light yellow powder. The crude product was dissolved in DCM and filtered over celite to remove any traces of the additional $ZnBr_2$, evaporated and dried in vacuo to obtain **3a** as a yellow powder. Yield: 210 mg (78%). IR: B-H 2562 cm^{-1}.
^{1}H NMR (300 MHz, $CDCl_3$) δ (ppm): 8.86 (d, J=9.3Hz, 1H, ArH), 8.59 (d, J=9.0Hz, 1H, ArH), 8.33 (d, J=9.3Hz, 1H, ArH), 7.36 (d, J=9.3Hz, 1H, Ar), 7.25 (d, J=9.0Hz, 1H, Ar), 7.01 (d, J=9.3Hz, 1H, Ar), 5.88 (bs, 1H, BH), 3.84 (m, 4H, THF), 1.89 (m, 4H, THF), 1.10 (s, 9H, CH_3), 1.03 (s, 9H, CH_3), 0.92 (s, 9H, CH_3).
^{13}C NMR (300 MHz, $CDCl_3$) δ (ppm): 175.57 (Ar-**C**), 174.92 (Ar-**C**), 173.68 (Ar-**C**), 163.29 (Ar-**C**), 162.68 (Ar-**C**), 162.49 (Ar-**C**), 140.40 (Ar-**C**), 139.77 (Ar-**C**), 138.37 (Ar-**C**), 124.95 (Ar-**C**), 124.39 (Ar-**C**), 123.92 (Ar-**C**), 68.64 (O-**C**H_2), 36.69 (R-**C**-$(CH_3)_3$), 36.62 (R-**C**-$(CH_3)_3$), 29.07 (R-**C**-$(CH_3)_3$), 29.04 (R-C-(**C**$H_3)_3$), 28.91 (R-C-(**C**$H_3)_3$), 25.74 (CH_2-**C**H_2). M^+ calc.: 1237.194 m/z. found: 1237.199 m/z.
Upon standing under inert atmosphere, the solution turned blue and the complex **3b** was obtained. ^{1}H NMR (300 MHz, $CDCl_3$) δ (ppm): 8.94 (d, J=9.1Hz, 1H, ArH), 8.69 (d, J=9.1Hz, 1H, ArH), 8.28 (d, J=9.0Hz, 1H, ArH), 7.39 (d, J=9.0Hz, 1H, Ar), 7.25 (d, J=9.1Hz, 1H, Ar), 7.02 (d, J=9.1Hz, 1H, Ar), 5.85 (bs, 1H, BH), 1.13 (s, 9H, CH_3), 1.05

(s, 9H, CH_3), 0.93 (s, 9H, CH_3).
^{13}C NMR (300 MHz, $CDCl_3$) δ (ppm): 175.76 (Ar-**C**), 174.85 (Ar-**C**), 173.27 (Ar-**C**), 163.34 (Ar-**C**), 163.03 (Ar-**C**), 162.62 (Ar-**C**), 140.96 (Ar-**C**), 138.93 (Ar-**C**), 138.90 (Ar-**C**), 124.55 (Ar-**C**), 124.24 (Ar-**C**), 123.98 (Ar-**C**), 36.88 (R-**C**-$(CH_3)_3$), 36.70 (R-**C**-$(CH_3)_3$), 36.67 (R-**C**-$(CH_3)_3$), 29.18 (R-C-(**C**$H_3)_3$), 29.10 (R-C-(**C**$H_3)_3$), 28.96 (R-C-(**C**$H_3)_3$).

3.3.2. [ZnI(Tn^{tBu})(THF)] (4)

Under inert atmosphere and light exclusion, 200 mg (1.0 equiv, 0.37 mmol) of **1** were mixed with 190 mg (1.5 equiv. 0.56 mmol) of ZnI_2 and dissolved in 5 mL of dry THF. After stirring for 16 h, the beige solution was evaporated to give a light yellow powder. The crude product was dissolved in DCM, to remove any traces of the additional ZnI_2, evaporated and dried in vacuo to obtain **4** as a yellow powder. Yield: 195 mg (68%). IR: B-H 2565 cm^{-1}
^{1}H NMR (300 MHz, $CDCl_3$) δ (ppm): 8.97 (d, J=9.1Hz, 3H, ArH), 7.43 (d, J=9.1Hz, 3H, ArH), 6.23 (bs, 1H, BH), 3.99 (m, 4H, THF), 1.96 (m, 4H, THF), 0.98 (s, 27H, CH_3).
^{13}C NMR (300 MHz, $CDCl_3$) δ (ppm): 174.34 (Ar-**C**), 164.13 (Ar-**C**), 138.65 (Ar-**C**), 125.25 (Ar-**C**), 69.63 (O-**C**H_2), 36.79 (R-**C**-$(CH_3)_3$), 28.92 (R-C-(**C**$H_3)_3$), 25.55 (CH_2-**C**H_2). M^+ calc.: 1285.180 m/z. found: 1285.187 m/z.

3.3.3. [ZnI(Tn^{tBu})] (5)

Under inert atmosphere and light exclusion, 200 mg (1.0 equiv, 0.37 mmol) of **1** were mixed with 190 mg (1.5 equiv, 0.56 mmol) of ZnI_2 and dissolved in 5 mL of dry DCM. After stirring for 16 h, the beige solution was filtered over celite and evaporated to give a light green powder. Yield: 180 mg (62%).
^{1}H NMR (300 MHz, $CDCl_3$) δ (ppm): 8.94 (d, J=9.13Hz, 1H, ArH), 8.72 (d, J=9.13Hz,

1H, ArH), 8.28 (d, J=9.01Hz, 1H, ArH), 7.39 (d, J=9.13Hz, 1H, Ar), 7.25 (d, J=9.01Hz, 1H, Ar), 7.02 (d, J=9.13Hz, 1H, Ar), 5.87 (bs, 1H, BH), 1.13 (s, 9H, CH_3), 1.05 (s, 9H, CH_3), 0.93 (s, 9H, CH_3). Re-dissolving the green powder in THF and subsequent evaporation yielded a yellow powder. ^{1}H NMR (300 MHz, $CDCl_3$) δ (ppm): 8.94 (d, J=9.39Hz, 1H, ArH), 8.69 (d, J=9.13Hz, 1H, ArH), 8.27 (d, J=9.13Hz, 1H, ArH), 7.42 (d, J=9.13Hz, 1H, Ar), 7.28 (d, J=9.39Hz, 1H, Ar), 7.02 (d, J=9.13Hz, 1H, Ar), 5.88 (bs, 1H, BH), 3.97 (m, 4H, THF), 1.93 (m, 4H, THF), 1.13 (s, 9H, CH_3), 1.05 (s, 9H, CH_3), 0.92 (s, 9H, CH_3).

3.3.4. [ZnBr(^{Pn}Bm)] (6)

200 mg (1.0 equiv, 0.47 mmol) of Na(^{Pn}Bm)] were dissolved in 15 mL of dry DCM. To the beige solution, 105 mg (1.0 equiv, 0.47 mmol)of anhydrous zinc bromide was added and stirred at room temperature for 16 h. The beige suspension was filtered and dried in vacuo to obtain **6** as a white powder. Yield: 212 mg (82%).
^{1}H NMR (300 MHz, DMSO-d6) δ (ppm): 7.57 (d, J=9.13Hz, 1H, ArH), 7.33 (d, J=9.13Hz, 1H, ArH), 7.24 (s, 2H, ArH), 6.79 (s, 2H, ArH), 5.29 (bs, 1H, BH), 3.50 (s, 6H, N-CH_3), 1.13 (s, 9H, CH_3).
^{13}C NMR (300 MHz, DMSO-d6) δ (ppm): 153.75 (Ar-**C**), 141.93 (Ar-**C**), 122.29 (Ar-**C**), 122.06 (Ar-**C**), 121.41 (Ar-**C**), 120.66 (Ar-**C**), 36.36 (R-C-(**C**H_3)$_3$), 34.66, 28.65 (R-C-(**C**H_3)$_3$).
Elemental Anal. calc: C: 28.00, H: 3.48, N: 10.00, found: C: 28.31, H: 3.47, N: 10.77. Crystal structure and crystallographic data are given in the appendix.

3.3.5. [Fe(Tn^{tBu})(OTf)] (7)

In 10 mL of dry diethyl ether, 100 mg (1.0 equiv, 0.19 mmol) of **1** and 80 mg (1.2 equiv, 0.22 mmol) of $Fe(OTf)_2$ were suspended. The orange suspension was stirred under inert atmosphere for 24 h. The resulting orange precipitate was centrifugated twice for 15 min and 2000 rpm. The light yellow solution was transferred into another flask, while the

orange precipitate was dried in vacuo to obtain **7** as a light red powder. Yield: 140 mg (94%) IR: B-H 2455 cm^{-1} M^+ calc.: 1287.244 m/z. found: 1287.238 m/z.

3.3.6. $[Fe(PnS_3Pn)_2](OTf)_2$ (8)

Under inert atmosphere, 550 mg (1 equiv, 1.5 mmol) of $Fe(OTf)_2$ and 800 mg (3.2 equiv, 4.76 mmol) of **PnH** were suspended in 10 mL of dry diethyl ether. Within 30 minutes, the brown suspension turned into a red, viscous suspension. After 16 hours, the precipitate was filtered and dried in vacuo, to obtain the product as a red solid. Yield: 730 mg (85% based on a 1:6 ratio). Elemental anal. calc: C: 34.40, H: 3.85, N: 8.91, found: C:34.43, H: 4.11, N: 8.89. Single crystals, suitable for X-ray diffraction could be obtained from a DCM solution. Figures of the crystal structure and crystallographic data are given in the appendix.

Appendix A.

Supplementary data

IR-spectra

IR spectrum of PnH

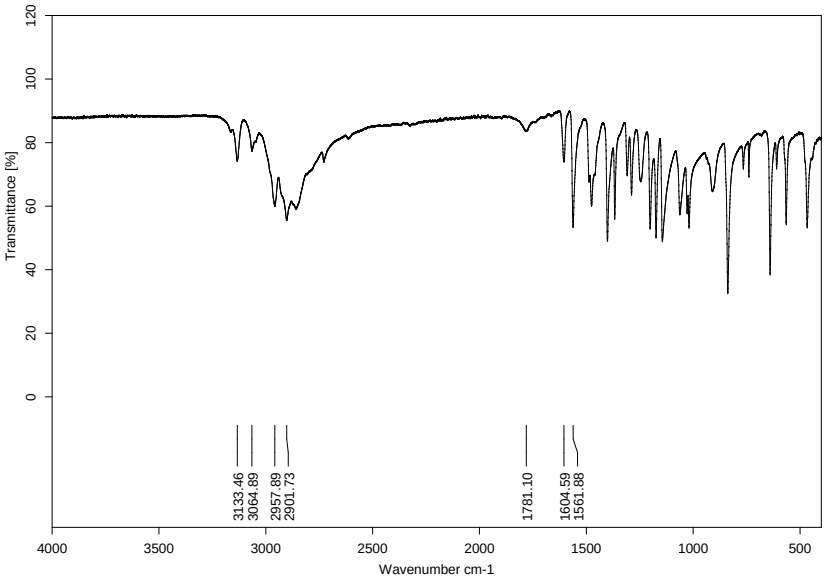

Figure A.1.: IR-spectrum of **PnH**.

IR spectrum of 1

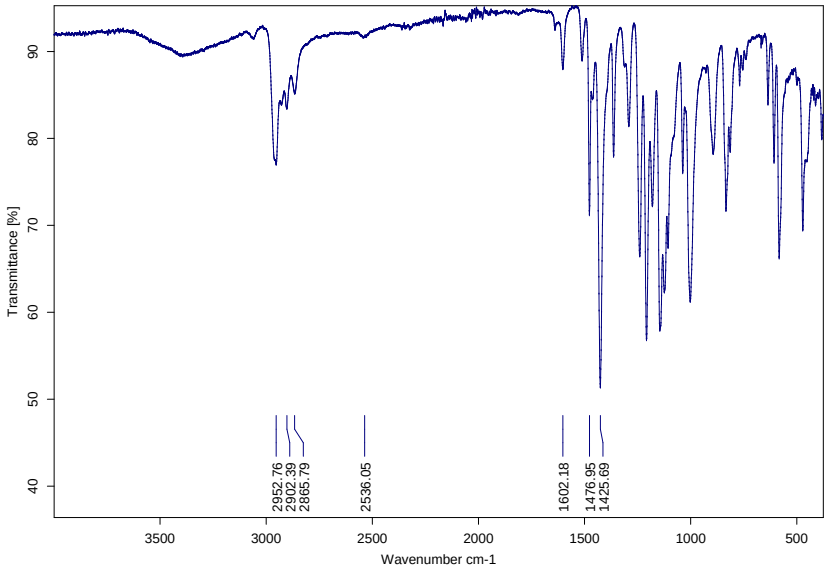

Figure A.2.: IR-spectrum of **1**.

IR spectrum of 2

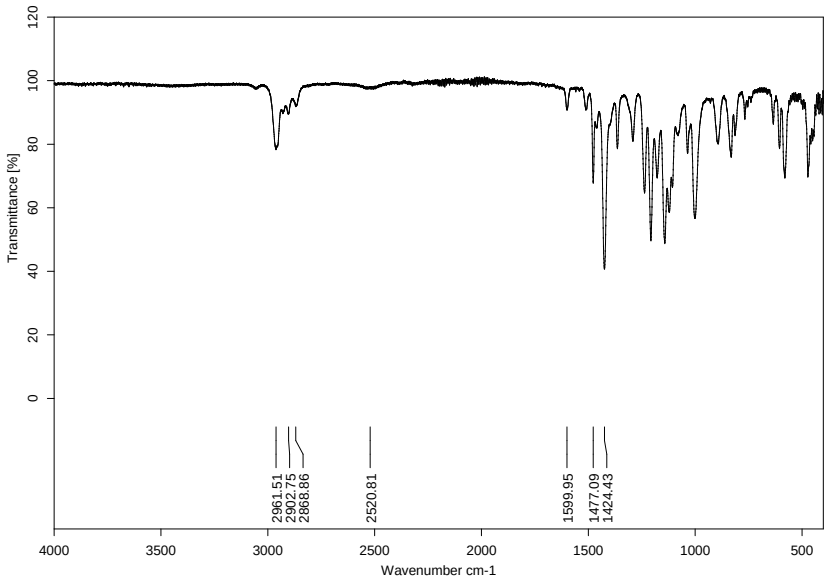

Figure A.3.: IR-spectrum of **2**.

IR spectrum of 3

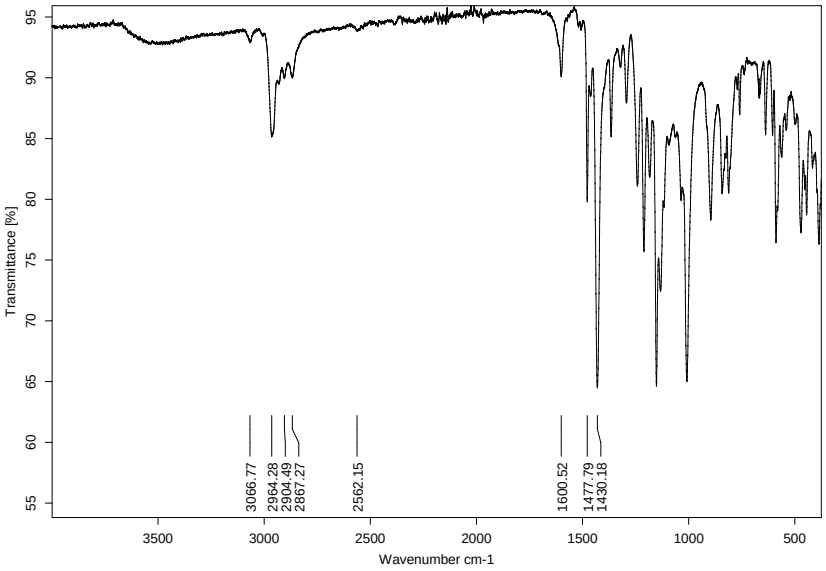

Figure A.4.: IR-spectrum of **3**.

IR spectrum of 4

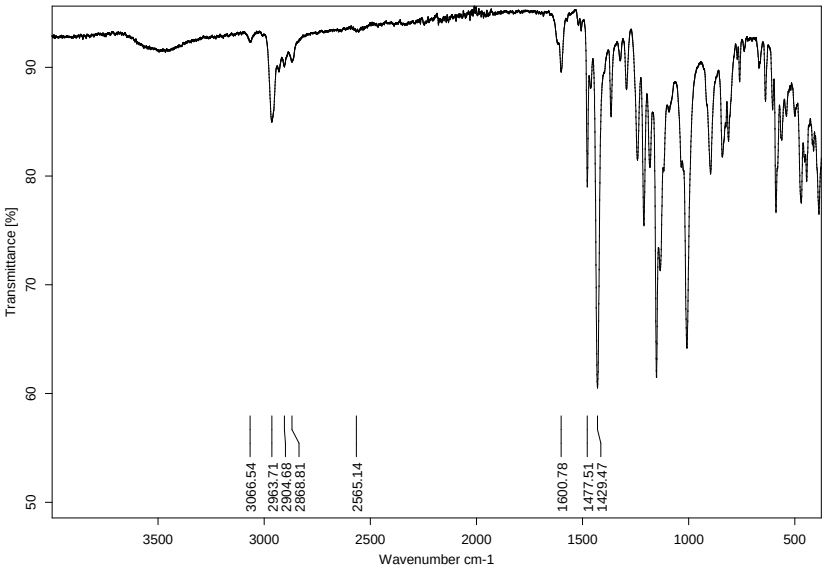

Figure A.5.: IR-spectrum of **4**.

IR spectrum of 7

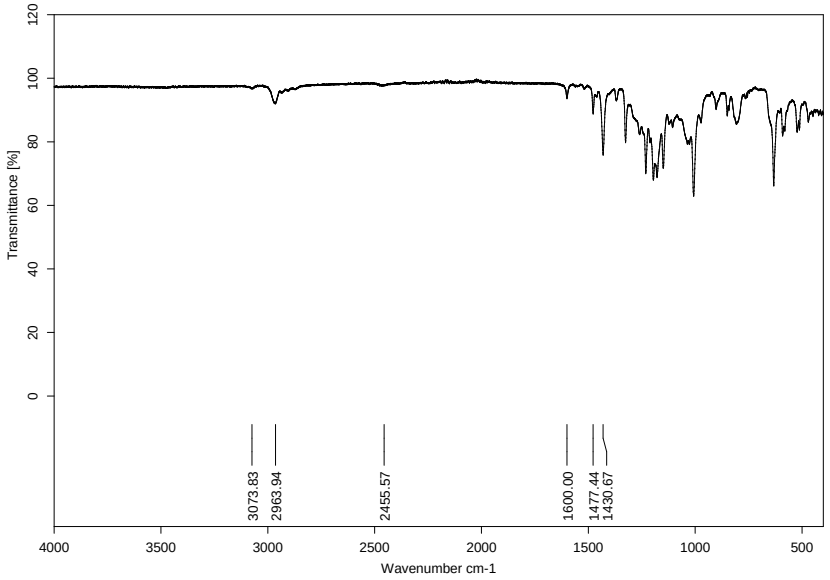

Figure A.6.: IR-spectrum of **7**.

IR spectrum of 8

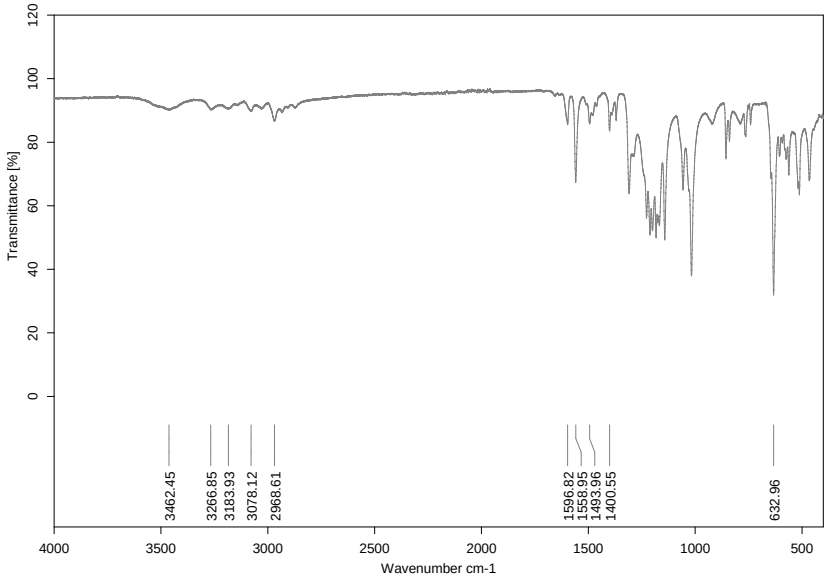

Figure A.7.: IR-spectrum of **8**.

High-resolution mass

High-resolution mass of 2

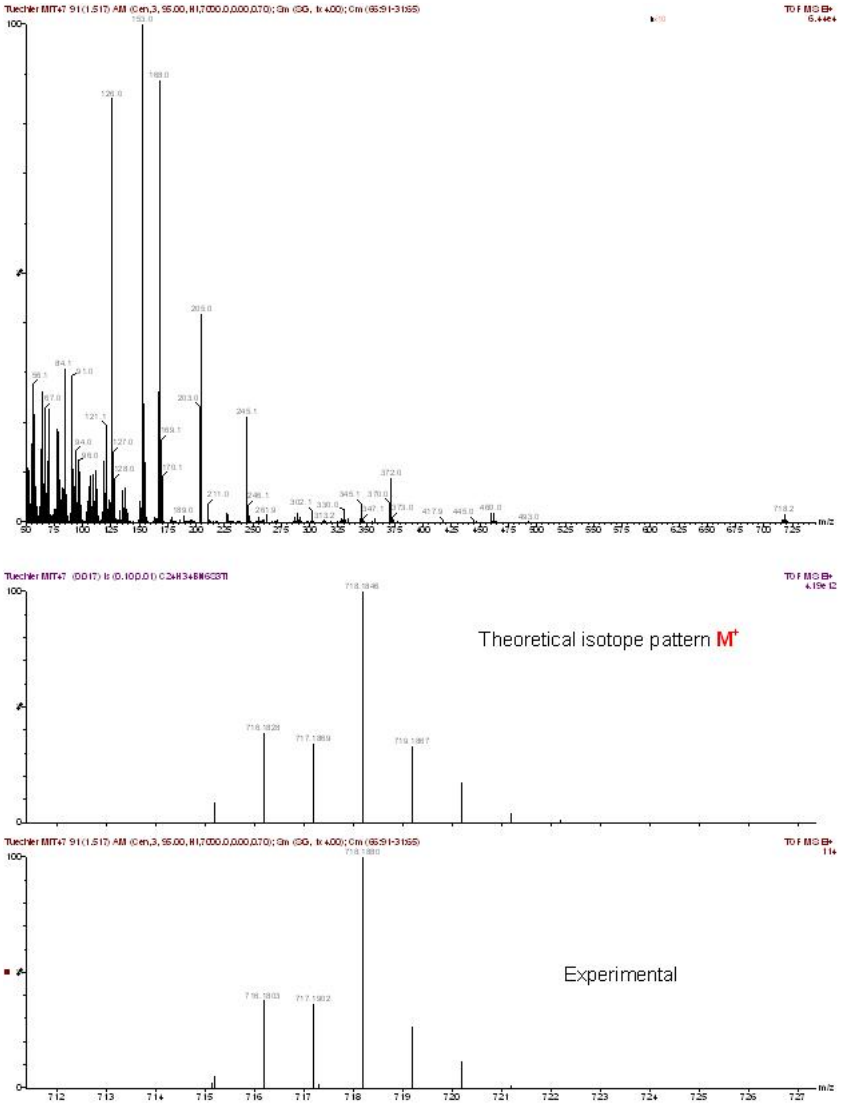

Figure A.8.: high-resolution mass isotope pattern of **2**.

High-resolution mass of 3

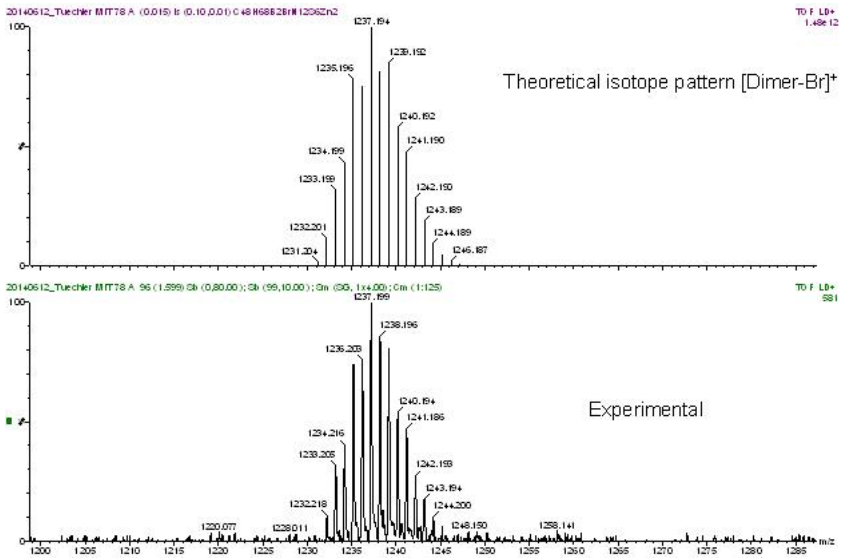

Figure A.9.: high-resolution mass isotope pattern of **3**.

High-resolution mass of 4

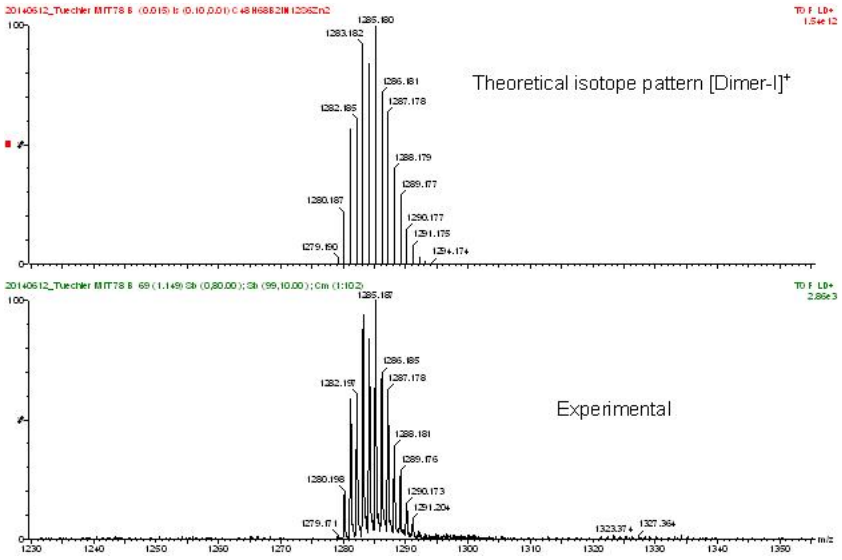

Figure A.10.: high-resolution mass isotope pattern of **4**.

High-resolution mass of 8

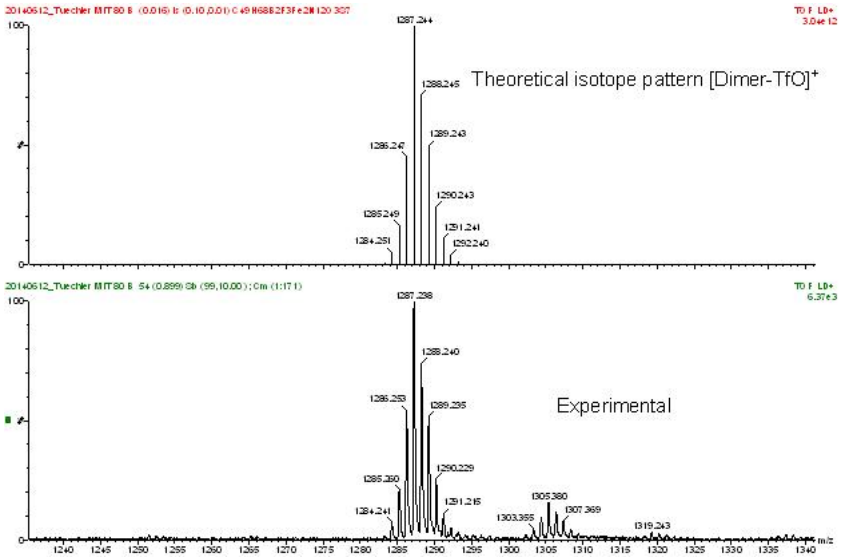

Figure A.11.: high-resolution mass isotope pattern of **7**.

Crystallographic data

6- tert- butyl- 3-thiopyridazine (PnH)

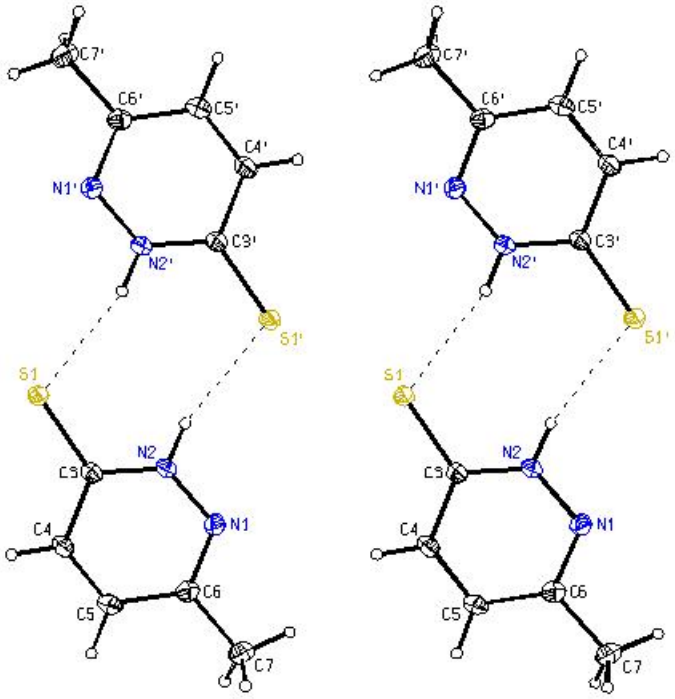

Figure A.12.: stereoscopic ORTEP plot of **PnH** showing the atomic numbering scheme. The probability ellipsoids are drawn at the 50% probability level. The H atoms are drawn with arbitrary radii, the hydrogen bonds are indicated by dashed lines.

The non-hydrogen atoms were refined with anisotropic displacement parameters without any constraints. The H atom of the NH group was put at the external bisector of the C–N–N angle at a N–H distance of 0.88 Å but the isotropic displacement parameter was free to refine. The H atoms bonded to C of the pyridazinium ring were put at the external bisector of the C–C–C angles at C–H distances of 0.95 Å and a common isotropic displacement parameter was refined for these H atoms. The H atoms of the methyl group were refined with common isotropic displacement parameters and idealized geometry with tetrahedral angles, enabling rotation around the C–C bond, and C–H distances of 0.98 Å.

Table A.1.: crystallographic data and structure refinement for **PnH**.

Empirical formula	$C_5H_6N_2S$
Formula weight	126.18
Crystal description	needle, yellow
Crystal size	0.34 x 0.32 x 0.07mm
Crystal system, space group	orthorhombic, P b c n
Unit cell dimensions	
a	8.2980(3)Å
b	11.8267(4)Å
c	12.1382(3)Å
Volume	1191.22(7)Å^3
Z	8
Calculated density	1.407Mg/m^3
F(000)	528
Linear absorption coefficient μ	0.425mm^{-1}
Reflections collected / unique	8985 / 1744
Significant unique reflections	1557 with I $> 2\sigma$(I)
R(int), R(sigma)	0.0191, 0.0138
Data / parameters / restraints	1744 / 77 / 0
Goodness-of-fit on F^2	1.038
Final R indices [I $> 2\sigma$(I)]	R1 = 0.0286, wR2 = 0.0793
R indices (all data)	R1 = 0.0321, wR2 = 0.0825
Largest difference peak and hole	0.498 and -0.194e/Å^3

Table A.2.: full list of bond lengths [Å] and angles [°] for **PnH**.

S(1)-C(3)	1.6926(10)	C(3)-C(4)-H(4)	120.1
N(1)-C(6)	1.3154(14)	C(4)-C(5)-C(6)	119.72(9)
N(1)-N(2)	1.3552(12)	C(4)-C(5)-H(5)	120.1
N(2)-C(3)	1.3509(13)	C(6)-C(5)-H(5)	120.1
N(2)-H(2)	0.88	N(1)-C(6)-C(5)	121.25(10)
C(3)-C(4)	1.4302(13)	N(1)-C(6)-C(7)	116.76(9)
C(4)-C(5)	1.3570(15)	C(5)-C(6)-C(7)	121.99(9)
C(4)-H(4)	0.95	C(6)-C(7)-H(71)	109.5
C(5)-C(6)	1.4300(15)	C(6)-C(7)-H(72)	109.5
C(5)-H(5)	0.95	H(71)-C(7)-H(72)	109.5
C(6)-C(7)	1.4986(14)	C(6)-C(7)-H(73	109.5
C(7)-H(71)	0.98	H(71)-C(7)-H(73)	109.5
C(7)-H(72)	0.98	H(72)-C(7)-H(73)	109.5
C(7)-H(73)	0.98	C(6)-N(1)-N(2)-C(3)	-0.30(15)
C(6)-N(1)-N(2)	116.93(9)	N(1)-N(2)-C(3)-C(4	0.93(14)
C(3)-N(2)-N(1)	127.53(8)	N(1)-N(2)-C(3)-S(1)	-177.77(8)
C(3)-N(2)-H(2)	116.2	N(2)-C(3)-C(4)-C(5)	-0.86(14)
N(1)-N(2)-H(2)	116.2	S(1)-C(3)-C(4)-C(5)	177.81(8)
N(2)-C(3)-C(4)	114.81(9)	C(3)-C(4)-C(5)-C(6)	0.25(15)
N(2)-C(3)-S(1)	121.18(7)	N(2)-N(1)-C(6)-C(5)	-0.43(15)
C(4)-C(3)-S(1)	124.00(8)	N(2)-N(1)-C(6)-C(7)	179.96(9)
C(5)-C(4)-C(3)	119.75(9)	C(4)-C(5)-C(6)-N(1)	0.43(16)
C(5)-C(4)-H(4)	120.1	C(4)-C(5)-C(6)-C(7)	-179.97(10)

3,3'-disulfanediylbis(6-tert-butylpyridazine) (PnS_2)

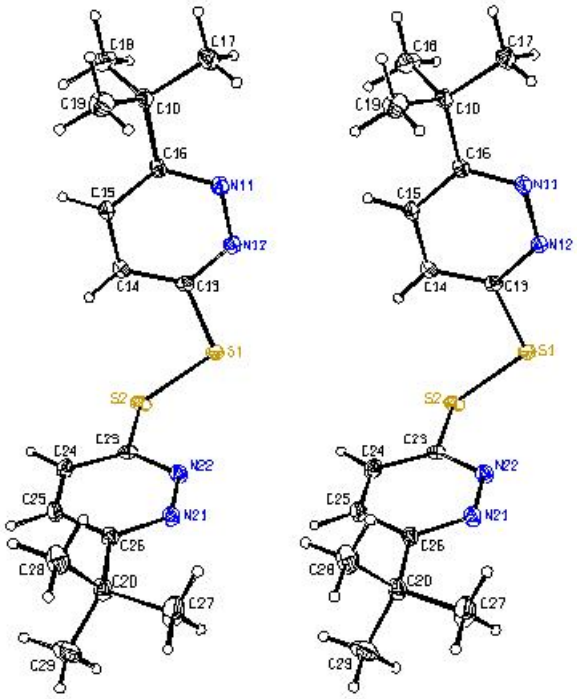

Figure A.13.: stereoscopic ORTEP plot of the disulfide showing the atomic numbering scheme. The probability ellipsoids are drawn at the 50% probability level. The H atoms are drawn with arbitrary radii.

The H atoms of the pyridazine rings were put at the external bisectors of the C–C–C angles at C–H distances of 0.95 Å and common isotropic displacement parameters were refined for the H atoms of the same phenyl group. The H atoms of the methyl groups were refined with common isotropic displacement parameters for the H atoms of the same group and idealized geometries with tetrahedral angles, enabling rotation around the C–C bond, and C–H distances of 0.98 Å.

Table A.3.: crystallographic data and structure refinement for $\mathbf{PnS_2}$.

Empirical formula	$C_{16}H_{22}N_4S_2$
Formula weight	334.50
Crystal description	needle, colorless
Crystal size	0.33 x 0.17 x 0.05mm
Crystal system, space group	triclinic, P-1
Unit cell dimensions	
a	5.82840(10)Å
b	11.5363(3)Å
c	13.7476(3)Å
α	107.9297(10)°
β	95.8257(9)°
γ	95.3949(9)°
Volume	867.23(3)Å^3
Z	2
Calculated density	1.281Mg/m^3
F(000)	356
Linear absorption coefficient μ	0.309mm^{-1}
Reflections collected / unique	9787 / 5038
Significant unique reflections	4216 with I $> 2\sigma$(I)
R(int), R(sigma)	0.0214, 0.0323
Data / parameters / restraints	5038 / 213 / 0
Goodness-of-fit on F^2	1.038
Final R indices [I $> 2\sigma$(I)]	R1 = 0.0346, wR2 = 0.0859
R indices (all data)	R1 = 0.0449, wR2 = 0.0909
Largest difference peak and hole	0.546 and -0.281e/Å^3

Table A.4.: selected bond lengths [Å] and angles [°] for $\mathbf{PnS_2}$.

S(1)-C(13)	1.7789(12)	N(22)-C(23)	1.3256(16)
S(1)-S(2)	2.0264(4)	C(13)-S(1)-S(2)	104.71(4)
N(11)-C(16)	1.3348(15)	N(12)-C(13)-S(1)	109.96(9)
N(11)-N(12)	1.3560(14)	C(14)-C(13)-S(1)	126.18(9)
N(12)-C(13)	1.3253(15)	C(23)-S(2)-S(1)	103.79(4)
S(2)-C(23)	1.7901(12)	N(22)-C(23)-S(2)	118.04(9)
N(21)-C(26)	1.3353(15)	C(24)-C(23)-S(2)	118.09(9)
N(21)-N(22)	1.3526(14)		

bis((μ³-oxo)-bis(μ³3-6-tert-butylpyridazine-3-sulfinato-N,O,O')-chloro-di-zinc(II))

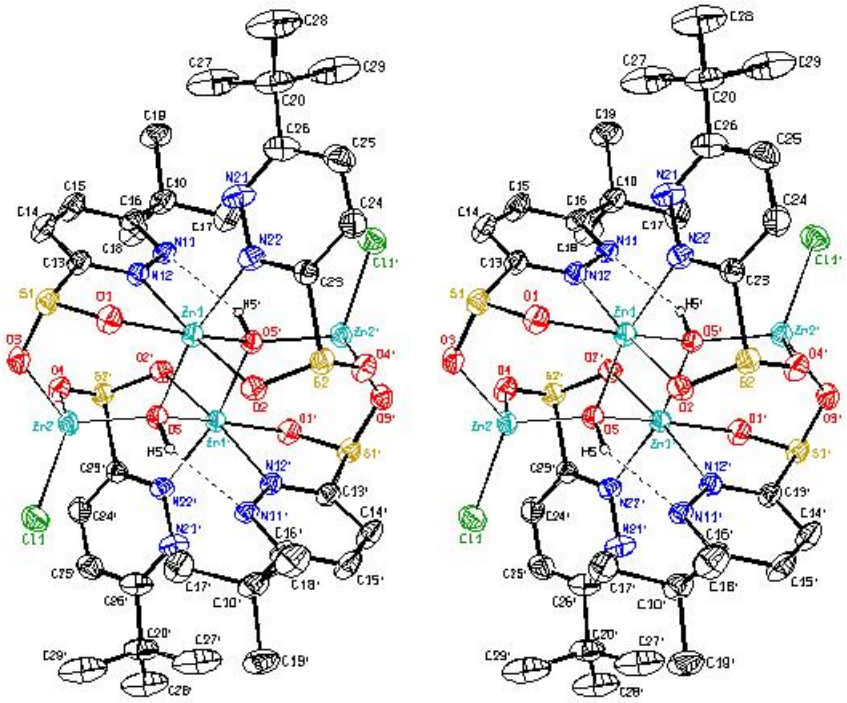

Figure A.14.: stereoscopic ORTEP plot of the centro-symmetric complex of the decomposition product showing the atomic numbering scheme. The probability ellipsoids are drawn at the 50% probability level. The disordered solvent molecules and the less occupied orientations of the disordered tert. butyl groups as well as the H atoms were omitted for clarity reasons. The H atoms of the OH groups were drawn with arbitrary radii and the intra-molecular hydrogen bonds were indicated by dashed lines.

The solvent molecule situated in a large void of approx. 178 Å^3 is disordered over two orientations around a centre of symmetry. Their non-hydrogen atoms were refined with isotropic displacement parameters with site occupation factors of 0.5. The equivalent bonds in the THF molecule were restrained to have the same lengths and the H atoms of the CH_2 groups were included at calculated positions with approximately tetrahedral angles and C–H distances of 0.99 Å with their isotropic displacement parameters fixed to 1.2 times U_{eq} of the C atom they are bonded to. The tert. butyl group bonded to

C26 was disordered over two orientations and was refined with site occupation factors of 0.686(5) and 0.314(5), respectively. The same anisotropic displacement parameters were used for equivalent C atoms of the disordered tert. butyl group. The other non-hydrogen atoms were refined with anisotropic displacement parameters without any constraints. The H atoms of the disordered methyl groups were refined with idealized geometries with tetrahedral angles, staggered conformations, and C–H distances of 0.98 Å. Their isotropic displacement parameters were fixed to 1.3 times U_{eq} of the C atom they are bonded to. The H atoms of the ordered methyl groups were refined with common isotropic displacement parameters for the H atoms of the same group and idealized geometries with tetrahedral angles, enabling rotation around the C–C bond, and C–H distances of 0.98 Å. The H atoms of the pyridazine rings were put at the external bisectors of the C–C–C angles at C–H distances of 0.95 Å and common isotropic displacement parameters were refined for the H atoms of the same ring. After the refinement of all other atoms the position of the H atom of the OH group could be taken from a difference Fourier map. The O–H distance was fixed to 0.84 Å, and the H atom was refined with an individual isotropic displacement parameter without any constraints to the bond angles.

Table A.5.: crystallographic data and structure refinement.

Empirical formula	$C_{32}H_{46}C_{l2}N_8O_{10}S_4Zn_4$ * C_4H_8O
Formula weight	1235.49
Crystal description	block, colorless
Crystal size	0.24 x 0.13 x 0.10mm
Crystal system, space group	monoclinic, P 2_1/n
Unit cell dimensions	
a	11.8257(3)Å
b	14.5199(4)Å
c	15.3873(4)Å
β	97.1970(10)°
Volume	2621.31(12)Å^3
Z	2
Calculated density	1.565Mg/m^3
F(000)	1264
Linear absorption coefficient μ	2.128mm^{-1}
Reflections collected / unique	26768 / 7654
Significant unique reflections	6488 with I $> 2\sigma$(I)
R(int), R(sigma)	0.0218, 0.0206
Data / parameters / restraints	7645 / 304 / 5
Goodness-of-fit on F^2	1.041
Final R indices [I $> 2\sigma$(I)]	R1 = 0.0359, wR2 = 0.0933
R indices (all data)	R1 = 0.0448, wR2 = 0.1000
Largest difference peak and hole	1.075 and -0.748e/Å^3

Table A.6.: selected bond lengths [Å] and angles [°].

Zn(1)-O(5)	2.0575(12)	O(3)-Zn(2)-O(4)	100.05(6)
Zn(1)-O(2)	2.0914(14)	O(5)-Zn(2)-Cl(1)	110.84(3)
Zn(1)-O(1)	2.1162(14)	O(3)-Zn(2)-Cl(1)	112.58(5)
Zn(1)-N(12	2.1287(16)	O(4)-Zn(2)-Cl(1)	115.93(5)
Zn(1)-N(22)	2.1383(18)	O(1)-S(1)-O(3)	109.88(9)
Zn(1)-O(5)	2.1418(10)	O(1)-S(1)-C(13)	100.78(9)
Zn(2)-O(5)	1.9381(12)	O(3)-S(1)-C(13)	99.59(9)
Zn(2)-O(3)	1.9807(15)	O(2)-S(2)-O(4)	110.22(9)
Zn(2)-O(4)	2.0007(15)	O(2)-S(2)-C(23)	100.46(9)
Zn(2)-Cl(1)	2.2054(6)	O(4)-S(2)-C(23)	98.81(9)
S(1)-O(1)	1.4992(16)	Zn(2)-O(5)-Zn(1)	118.92(5)
S(1)-O(3)	1.5285(17)	Zn(2)-O(5)-Zn(1)	118.00(5)
S(1)-C(13)	1.827(2)	Zn(1)-O(5)-Zn(1)	97.92(4)
S(2)-O(2)	1.5014(15)	Zn(2)-O(5)-H(5)	110.2(7)
S(2)-O(4)	1.5259(16)	Zn(1)-O(5)-H(5)	110.6(9)
S(2)-C(23)	1.817(2)	Zn(1)-O(5)-H(5)	99.1(5)
		O(5)-Zn(2)-O(4)	105.78(5)
O(2)-Zn(1)-N(12)	172.99(6)	S(1)-O(1)-Zn(1)	119.61(8)
O(5)-Zn(1)-N(22)	167.04(6)	S(2)-O(2)-Zn(1)	118.85(8)
O(1)-Zn(1)-O(5)	163.02(5)	S(1)-O(3)-Zn(2)	124.02(9)
O(5)-Zn(2)-O(3)	111.06(6)	S(2)-O(4)-Zn(2)	126.38(9)

bis(mu2-hydrogen-tris(3-mercapto-6-tert-butyl-pyridazin-2-yl)borato-S,S',S'')-di¬bromo-di-zinc(II)

(6)

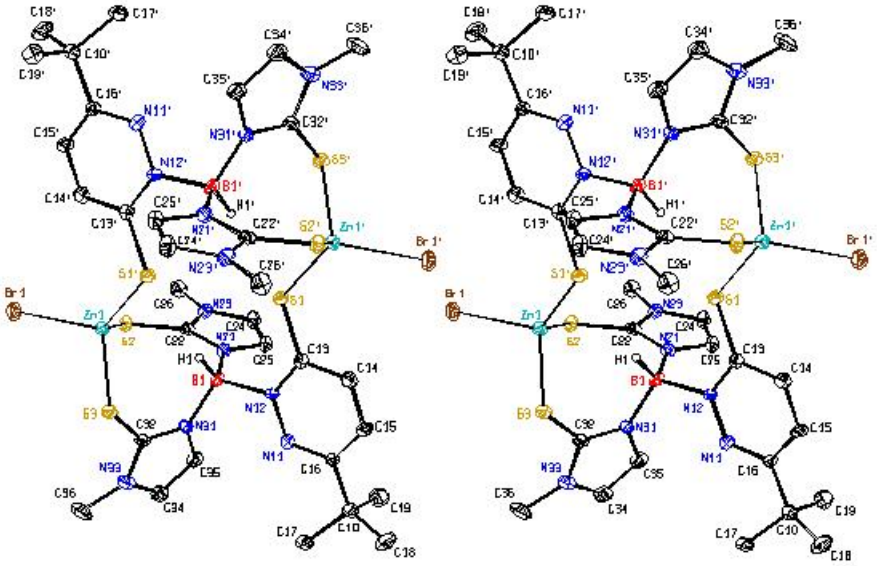

Figure A.15.: stereoscopic ORTEP plot of **6** showing the atomic numbering scheme. The probability ellipsoids are drawn at the 50% probability level. The H atoms are drawn with arbitrary radii.

The H atom H1 bonded to B1 was clearly identified in a difference Fourier map and was refined without any positional constraints with an isotropic displacement parameter. The H atoms bonded to ring atoms were put at the external bisectors of the C–C-X angles at C–H distances of 0.95 Å and common isotropic displacement parameters were refined for the H atoms of the same ring. The H atoms of the methyl groups were refined with common isotropic displacement parameters for the H atoms of the same group and idealized geometries with tetrahedral angles, enabling rotation around the X–C bond, and C–H distances of 0.98 Å.

Table A.7.: crystallographic data and structure refinement for **6**.

Empirical formula	$C_{32}H_{44}B_2Br_2N_{12}S_6Zn_2$ * $4C_7H_8$
Formula weight	1469.87
Crystal description	needle, colorless
Crystal size	0.22 x 0.12 x 0.07mm
Crystal system, space group	triclinic, P-1
Unit cell dimensions	
a	9.1011(6)Å
b	13.7402(10)Å
c	14.1721(10)Å
α	80.776(2)°
β	82.146(2)°
γ	72.062(3)°
Volume	1657.1(2)Å^3
Z	2
Calculated density	1.473Mg/m^3
F(000)	756
Linear absorption coefficient μ	2.166mm^{-1}
Reflections collected / unique	13201 / 6488
Significant unique reflections	4933 with I $> 2\sigma$(I)
R(int), R(sigma)	0.0322, 0.0566
Data / parameters / restraints	6488 / 402 / 0
Goodness-of-fit on F^2	1.040
Final R indices [I $> 2\sigma$(I)]	R1 = 0.0447, wR2 = 0.1211
R indices (all data)	R1 = 0.0674, wR2 = 0.1298
Largest difference peak and hole	0.923 and -0.578e/Å^3

Table A.8.: selected bond lengths [Å] and angles [°] for **6**.

Zn(1)-S(1)	2.3582(11)	N(11)-N(12)-B(1)	115.0(3)
Zn(1)-S(3)	2.3604(12)	C(22)-S(2)-Zn(1)	115.93(14)
Zn(1)-S(2)	2.3613(12)	C(22)-N(21)-C(25)	107.7(3)
Zn(1)-Br(1)	2.4090(6)	C(22)-N(21)-B(1)	124.2(3)
B(1)-N(31)	1.537(6)	C(25)-N(21)-B(1)	128.1(3)
B(1)-N(21)	1.551(6)	C(32)-S(3)-Zn(1)	99.65(15)
B(1)-N(12)	1.585(5)	C(32)-N(31)-C(35)	107.9(3)
B(1)-H(1)	1.08(4)	C(32)-N(31)-B(1)	125.6(3)
S(1)-C(13)	1.711(4)	C(35)-N(31)-B(1)	126.4(4)
S(2)-C(22)	1.728(4)	Br(1)-Zn(1)-S(2)-C(22)	175.17(15)
S(3)-C(32)	1.719(4)	Br(1)-Zn(1)-S(3)-C(32)	118.93(14)
S(1)-Zn(1)-S(3)	102.21(4)	S(1)-Zn(1)-S(2)-C(22)	49.83(16)
S(1)-Zn(1)-S(2	117.39(4)	S(3)-Zn(1)-S(2)-C(22)	-71.03(16)
S(3)-Zn(1)-S(2)	115.63(4)	S(1)-Zn(1)-S(3)-C(32)	-118.33(14)
S(1)-Zn(1)-Br(1)	116.21(3)	S(2)-Zn(1)-S(3)-C(32)	10.41(15)
S(3)-Zn(1)-Br(1)	107.31(3)	Zn(1)-S(1)-C(13)-N(12)	173.5(3)
S(2)-Zn(1)-Br(1)	98.32(3)	Zn(1)-S(1)-C(13)-C(14)	-8.4(4)
N(31)-B(1)-N(21)	108.5(3)	Zn(1)-S(2)-C(22)-N(21)	23.7(4)
N(31)-B(1)-N(12)	111.5(3)	Zn(1)-S(2)-C(22)-N(23)	-156.8(3)
N(21)-B(1)-N(12)	108.5(3)	Zn(1)-S(3)-C(32)-N(33)	-126.0(3)
N(31)-B(1)-H(1)	110(2)	C(13)-S(1)-Zn(1)	114.57(14)
N(21)-B(1)-H(1)	113(2)	C(13)-N(12)-N(11)	123.0(3)
N(12)-B(1)-H(1)	106(2)	C(13)-N(12)-B(1)	122.0(3)

bis[3,3'-trisulfane-1,3-diylbis(6-tert-butylpyridazine)-N,S,S']iron(II) di(trifluorome-thanesulfonate) (8)

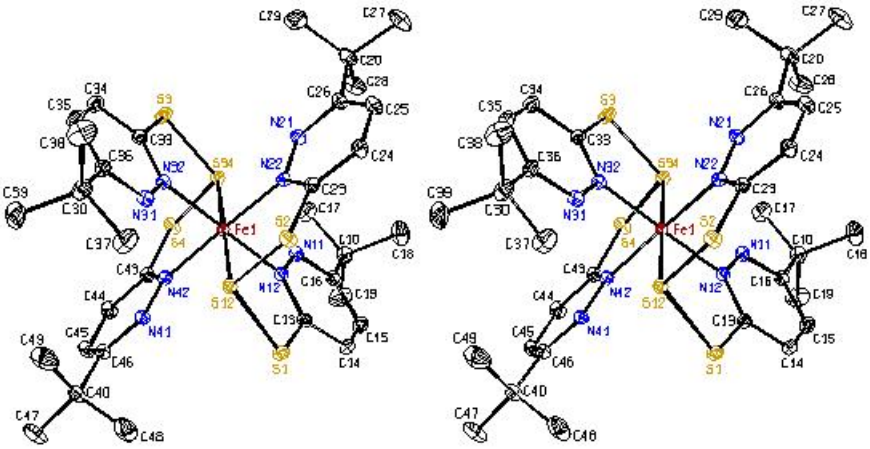

Figure A.16.: stereoscopic ORTEP plot of **8** showing the atomic numbering scheme. The probability ellipsoids are drawn at the 50% probability level. The H atoms and the OTf groups are omitted for clarity.

The structure could not be solved by direct methods, but by interpretation of the patterson map and subsequent structure expansion (SHELXS-97)[115]. Several attempts with different superposition vectors had to be made to overcome the pseudo-symmetry problem and to get a correct solution. Full-matrix least-squares refinements of F^2 values against all reflections were performed by (SHELXL-97)[115]. The non-hydrogen atoms were refined with anisotropic displacement parameters without any constraints. The H atoms of the pyridazine rings were put at the external bisectors of the C–C–C angles at C–H distances of 0.95 Å and common isotropic displacement parameters were refined for the H atoms of the same ring. The H atoms of the methyl groups were refined with common isotropic displacement parameters for the H atoms of the same group and idealized geometries with tetrahedral angles, enabling rotation around the C–C bond, and C–H distances of 0.98 Å. The H atoms of the solvent molecules were refined with common isotropic displacement parameters for the H atoms of the same group and idealized geometry with approximately tetrahedral angles and C–H distances of 0.99 Å.

Table A.9.: crystallographic data and structure refinement for **8**.

Empirical formula	$C_{32}H_{44}FeN_8S_6^{+2}$ $(CF_3SO_3S^{\breve{}})_2$ * $3CH_2Cl_2$
Formula weight	1341.88
Crystal description	block, orange
Crystal size	0.32 x 0.25 x 0.21mm
Crystal system, space group	monoclinic, P 2_1/c
Unit cell dimensions	
a	15.2993(4)Å
b	14.6458(4)Å
c	50.0036(13)Å
β	96.2896(9)°
Volume	11136.9(5)Å^3
Z	8
Calculated density	1.601Mg/m^3
F(000)	5488
Linear absorption coefficient μ	0.929mm^{-1}
Reflections collected / unique	96005 / 32325
Significant unique reflections	23702 with I $> 2\sigma$(I)
R(int), R(sigma)	0.0260, 0.0361
Data / parameters / restraints	32325 / 1362 / 0
Goodness-of-fit on F^2	1.030
Final R indices [I $> 2\sigma$(I)]	R1 = 0.0372, wR2 = 0.0865
R indices (all data)	R1 = 0.0580, wR2 = 0.0931
Largest difference peak and hole	0.903 and -0.715e/Å^3

Table A.10.: selected bond lengths [Å] and angles [°] for **8**.

Fe(1)-N(22)	1.9700(14)	S(1)-S(12)-Fe(1)	101.79(2)
Fe(1)-N(32)	1.9701(14)	C(13)-S(1)-S(12)	101.05(6)
Fe(1)-N(12)	1.9724(14)	C(13)-N(12)-N(11)	119.85(13)
Fe(1)-N(42)	1.9765(14)	C(13)-N(12)-Fe(1)	125.11(11)
Fe(1)-S(34)	2.2338(4)	N(11)-N(12)-Fe(1)	115.03(10)
Fe(1)-S(12)	2.2353(4)	C(23)-S(2)-S(12)	100.40(6)
S(1)-C(13)	1.7552(17)	C(23)-N(22)-N(21)	119.76(13)
S(1)-S(12)	2.0831(6)	C(23)-N(22)-Fe(1)	125.58(11)
S(12)-S(2)	2.0743(6)	N(21)-N(22)-Fe(1)	114.64(10)
S(2)-C(23)	1.7527(16)	S(3)-S(34)-S(4)	103.67(2)
S(3)-C(33)	1.7573(17)	S(3)-S(34)-Fe(1)	102.63(2)
S(3)-S(34)	2.0780(6)	S(4)-S(34)-Fe(1)	102.38(2)
S(34)-S(4)	2.0826(6)	C(33)-S(3)-S(34)	101.17(6)
S(4)-C(43)	1.7594(17)	C(33)-N(32)-N(31)	119.62(14)
N(12)-Fe(1)-N(32)	179.08(6)	C(33)-N(32)-Fe(1)	125.30(11)
N(22)-Fe(1)-N(42)	179.39(6)	N(31)-N(32)-Fe(1)	115.08(10)
S(12)-Fe(1)-S(34)	179.111(18)	C(43)-S(4)-S(34)	100.74(6)
S(2)-S(12)-S(1)	103.82(2)	C(43)-N(42)-Fe(1)	125.41(11)
S(2)-S(12)-Fe(1)	103.01(2)	N(41)-N(42)-Fe(1)	114.96(10)

Bibliography

[1] C.F. MIlls. *Zinc in Human Biology.* Springer-Verlag: New York, 1989.

[2] N.Krebs M. Hambidge. *J. Pediatr.*, 135:661–664, 1999.

[3] G.A. Eby. *J. Antimicrob. Chemother*, 40:483–493, 1997.

[4] A. Gadomski. *J. Am. Med. Assoc.*, 279:1999–2000, 1998.

[5] D.G. Barceloux. *J. Toxicol. Clin. Toxicol.*, 37:279–292, 1999.

[6] B.L: Vallee. *Zinc Enzymes.* Wiley: New York, 1983.

[7] D.S. Auld B.L. Vallee. *Matrix Metalloproteinases Inhib. Proc. Matrix Metalloproteinase Conf.*, pages 5–19, 1992.

[8] D.R. Williams. *Coord. Chem. Rev.*, 186:177–188, 1999.

[9] M.F. Dunn S. Rahuel-Clermont. *Copper Zinc Inflammatory Degener. Dis.*, pages 47–59, 1998.

[10] W.N. Lipscomb. *Annu. Rev. Biochem.*, 52:17–34, 1983.

[11] D.S. Auld. *Struct. Bonding*, 89:29–50, 1997.

[12] A. Glades B.L. Vallee. *Adv. Enzymol. Relat. Areas Mol. Biol.*, 56:283–430, 1984.

[13] P.Chakrabarti. *Protein Eng.*, 4:57–63, 1990.

[14] M.Dudev C. Lim. T.Dudev, Y.L.Lin. *J. Am. Chem. Soc.*, 125:3168–3180, 2003.

[15] R.B. Martin R.J. Sundberg. *Chem. Rev.*, 74:471–517, 1974.

[16] T.; Calimet Simonson. *N. Proteins*, 49:37–48, 2002.

[17] C. Dudev, T.; Lim. *J. Am. Chem. Soc.*, 124:6759–6766, 2002.

[18] D. S. Vallee, B. L.; Auld. *Acc. Chem. Res.*, 26:543–551, 1993.

[19] D. G. Maynard, A. T.; Covell. *J. Am. Chem. Soc.*, 123:1047–1058, 2001.

[20] S. Iuchi. *Cell. Mol. Life Sci.*, 58:625–635, 2001.

[21] Y. Berg, J. M.; Shi. *Science*, 271:1081–1085, 1996.

[22] S. Lindskog. *Pharmacol. Ther.*, 74:1–20, 1997.

[23] J. D. Christianson, D. W.; Cox. *Annu. Rev. Biochem.*, 68:33–57, 1999.

[24] K.; Ferry J. G. Tripp, B. C.; Smith. *J. Biol. Chem.*, 276:48615–48618, 2001.

[25] F. Meldrum, N. M.; Roughton. *J. Nature (London)*, 80:113–142, 1933.

[26] W. Koch E. Anders S. Sinnecker, M. Brauer. *Inorg. Chem.*, 40:1006, 2001.

[27] B.T. Storey F. Botre, G.Gros. *CarbonicAnhydrase*, VCH Publishers:Weinheim, 1991.

[28] L.M. Merz, K. M.; Banci. *J. Am. Chem. Soc.*, 119:863– 871, 1997.

[29] K. M.; van Eldik R.; Clark T. Hartmann, M.; Merz. *J. Mol. Model.*, 4:355–365, 1998.

[30] J. L.; Weston J.; Anders E. Brauer, M.; Perez-Lustres. *Inorg. Chem.*, 41:1454–1463, 2002.

[31] R. Vahrenkamp H. Alsfasser. *Chem. Ber.*, 126:695–701, 1993.

[32] E Kimura, E.; Kikuta. *J. Biol. Inorg. Chem.*, 5:139–155, 2000.

[33] M.; Liangnian Zongwan. *J. Prog. Chem.*, 14:311–317, 2002.

[34] J.; Walton P. H.; Ward M. D. Elsevier, C. J.; Reedijk. *Dalton*, pages 1869– 1880, 2003.

[35] H. Vahrenkamp. *Acc. Chem. Res.*, 32:589–596, 1999.

[36] P. G.; Balsky S. Jairam, R.; Potvin. *J. Chem. Soc., Perkin Trans.*, 2:363–367, 1999.

[37] S. P.; Lusby P. J.; Walton P. H. Cronin, L.; Foxon. *J. Biol. Inorg. Chem.*, 6:367–377, 2001.

[38] P. C.; Taylor P. C. Hannon, M. J.; Mayers. *Tetrahedron Lett.*, 39:8509–8512, 1998.

[39] N.; Ichikawa K.; Shiro M. Ibrahim, M. M.; Shimomura. *Inorg. Chim. Acta*, 313:125–136, 2001.

[40] I. E.; Hambley T. W. Zvargulis, E. S.; Buys. *Polyhedron*, 14:2267–2273, 1995.

[41] J.; Vahrenkamp H. Titze, C.; Hermann. *Chem. Ber.*, 128:1095–1103, 1995.

[42] S. Trofimenko. *J. Am. Chem. Soc.*, 88:1842–1844, 1966.

[43] A. Looney G. Parkin H. Vahrenkamp R. Alsfasser, S. Trofimenko. *Inorg. Chem.*, 30:4098–4100, 1991.

[44] K. McNeill G. Parkin Looney, R. Han. *J. Am. Chem. Soc.*, 115:4690–4697, 1993.

[45] G. Parkin W. Sattler. *Polyhedron*, 32:41–48, 2012.

[46] I. Cassidy M. D. Spicer A. R. Kennedy M. Garner, J. Reglinski. *Chem. Commun.*, 6:1975–1976, 1996.

[47] G.Parkin B.M. Bridgewater. *Inorg. Chem. Comm.*, 4:126–129, 2001.

[48] H. Vahrenkamp F. Gross. *Inorg. Chem.*, 44:3321–3329, 2005.

[49] G. Parkin C. Kimblin, T. Hascall. *Inorg. Chem.*, 36:5680–5681, 1997.

[50] B. Wu J. Seebacher H. Vahrenkamp M. Shu, R. Walz. *Eur. J. Inorg. Chem.*, pages 2502–2511, 2003.

[51] A.; Mitchell B.; Owen G. R. Dyson, G.; Hamilton. *Dalton Trans.*, page 6120, 2009.

[52] M. Zellerb A. D. Hunter M. Kumar, E. T. Papish. *Dalton Trans.*, 39:59–61, 2010.

[53] S.L. Schrier C. Camaschella. *Regulation of iron balance*, UpToDate:2011–11–07, 2011.

[54] S. Hong Y.M. Lee M. Clémancey R. Garcia-Serres T. Nomura T. Ogura J.M. Latour B. Hedman K.O. Hodgson W. Nam E.I. Solomon S.A. Wilson, J. Chen. *J. Am. Chem. Soc.*, 134:11791–11806, 2012.

[55] M.P. Jensen L. Que M. Costas, M.P. Mehn. *Chem. Rev.*, 104:939–986, 2004.

[56] M.V. Twigg J. Burgess. *Encyclopedia of inorganic chemistry: Iron: Inorganic and Coordination Chemistry*, Wiley, 2006.

[57] R.Y. Ho L. Que Jr. *Chem. Rev.*, 96:2607–2624, 1996.

[58] L. Que Jr. E. Hegg. *Eur. J. Biochem.*, 250:625–629, 1997.

[59] K.A.Pattridge W.C. Stallings J.A. Fee M.L. Ludwig M.S. Lah, M.M.Dixon. *Biochemistry*, 34:1646–1660, 1995.

[60] V. Fiilop K. Harlos G.J. Barton J. Hajdu-I. Andersson C.J. Schofield J.E. Baldwin P.L. Roach, I.J. Clifton. *Nature*, 375:700–704, 1995.

[61] L. Jr. Ito, M.; Que. *Angew. Chem., Int. Ed.*, 36:1342, 1997.

[62] K.; Hegg E. L.; Que L. Jr. Mehn, M. P.; Fujisawa. *J. Am. Chem. Soc.*, 125:7828, 2003.

[63] M. P.; Hegg E. L.; Liu A.; Ryle M. J.; Hausinger R. P.; Que L. Jr. Ho, R. Y. N.; Mehn. *J. Am. Chem. Soc.*, 123:5022, 2001.

[64] L. Que Jr. E.L. Hegg, R.Y.N Ho. *J. Am. Chem. Soc.*, 121:1972, 1999.

[65] N.; Amagai H.; Fukui H.; Moro-oka Y.; Mizutani Y.; Kitagawa T.; Mathur R.; Heerwegh K.; Reed C. A.; Randall C. R.; Que L. Jr. Tatsumi K. Kitajima, N.; Tamura. *J. Am. Chem. Soc.*, 116:9071, 1994.

[66] S.; Akita M.; Moro-oka Y. Ogihara, T.; Hikichi. *Inorg. Chem.*, 37:2614, 1998.

[67] J.M.Dunwell. *Biotechnol. Genet. Eng. Rev.*, 15:1, 1998.

[68] P.J.Gane J.M. Dunwell, S.Khuri. *Micorbiol. Mol. Biol. Rev.*, 64:153, 2000.

[69] W. A. Francisco M. R. Schaab, B. M. Barney. *Biochemistry*, 45:1009–1016, 2006.

[70] B. Nidetzky G. D. Straganz. *J. Am. Chem. Soc.*, 127:12306–12314, 2005.

[71] E. Bitto C. A. Bingman D. J. Aceti B. G. Fox G. N. Phillips Jr. J. G. McCoy, L. J. Bailey. *Proc. Natl. Acad. Sci*, 103:3084–3089, 2006.

[72] O. Griffith. *Methods in Enyzymology*, 143:366– 376, 1987.

[73] J. J. Banik I. Shalev J. L. Pinkham P. C. Uden M. J. Maroney S. C. Chai, A. A. Jerkins. *J. Biol. Chem.*, 280:9865–9869, 2005.

[74] L. Wei D. Tang P. Sun M. Bartlam Z. Rao S. Ye, X. Wu. *J. Biol. Chem.*, 2007:3391–3402, 282.

[75] Q. Huang Q. Hao T.P. Begley P.A. Karplus M.H. Stipanuk C.R. Simmons, Q. Liu. *J. Biol. Chem.*, 281:18723–18733, 2006.

[76] J.A. Sigman T.D. Pfister Y. Lu J.H. Dawson R. Perera, M. Sono. *Proc. Natl. Acad. Sci.*, 100:3641–3646, 2003.

[77] G.T. Babcock D.A. Proshlyakov, M.A. Pressler. *Proc. Natl. Acad. Sci.*, 95:8020–8025, 1998.

[78] M.J. Maroney S.C. Chai, J.R. Bruyere. *J. Biol. Chem.*, 281:15774–15779, 2006.

[79] L. Que Jr. M. Costas, K. Chen. *Coordination Chemistry Reviews*, 200–202:517–544, 2000.

[80] C. Limberg M. Merz L. Que Jr. T. Wistuba M. R. Bukowski, P. Comba. *Angew. Chem. Int. Ed.*, 43:1283–1283, 2004.

[81] D. P. Goldberg Y. M. Badiei, M. A. Siegler. *J. Am. Chem. Soc.*, 133:1274–1277, 2011.

[82] M. A. Siegler D. P. Goldberg A. C. McQuilken, Y. Jiang. *J. Am. Chem. Soc.*, 134:8758−8761, 2012.

[83] C. G.; Yang T.; Siegler M. A.; Troeppner O.; Jameson G. N. L.; Ivanovic-Burmazovic I.; Goldberg D. P Widger, L. R.; Davies. *J. Am. Chem. Soc.*, 136:2699–2702, 2014.

[84] D.W. Will P. Wohlfart G. Zoller, H. Strobel. *PCT Int. Appl.*, WO2008104279A1, 2008.

[85] C. Hammond D. Chin T. Durand-Reville, C. Jewell. *PCT Int. Appl.*, WO2008030579, 2008.

[86] J. Haiech M. Hibert J.-J. Bourguignon A. Velentza W. Hu M. Zasadzki D. M. Watterson, L. van Eldik. *PCT Int. Appl.*, WO2006050359, 2006.

[87] S. Trah R. Dumeunier C. Lamberth, S. V. Wendeborn. *PCT Int. Appl.*, WO2008089934, 2008.

[88] D. R. Lide. *CRC Handbook of Chemistry and Physics, 88th ed.*, Taylor & Francis:Boca Raton, 2007.

[89] P. V. Solntsev E. B. Rus-anov H. Krautscheid J. A. Howard A. N. Chernega K. V. Domasevitch, I. A. Gurałskiy. *Dalton Trans.*, page 3140–3148, 2007.

[90] P. G. Plieger S. Brooker, S. J. Hay. *Angew. Chem. Int. Ed.*, 39:1968–1970, 2000.

[91] D. H. Brown J. R. Allan, G. A. Barnes. *J. Inorg. Nucl. Chem.*, 33:3765–3771, 1971.

[92] S. Brooker M. Weitzer. *Dalton Trans.*, page 2448–2454, 2005.

[93] J. Fulara L. Lapinski, M. J. Nowak. *J. Phys. Chem.*, 96:6250–6254, 1992.

[94] I. Reva B. J. A. N. Almeida M. J. Nowak R. Fausto H. Rostkowska, L. Lapinski. *J. Phys. Chem. A*, 115:12142–12149, 2011.

[95] R. G. Pearson. *Inorganica Chimica Acta.*, 240:93–98, 1995.

[96] F.; Yu J.; Xu J. Wang, Y.; Bai. *Dalton Transactions*, 42:16547–16555, 2013.

[97] J.; Xu Y.; Mei Q.; Chen Q.; Leung W.; Zhang Q. Tong, B.; Qiang. *Journal of Solution Chemistry*, 41:1600–1609, 2012.

[98] P.; Vankatova H.; Vejsova M.; Ceslova L.; Padelkova Z.; Ruzicka A.; Holecek J. Ozerianskyi, A.; Svec. *Applied Organometallic Chemistry*, 25:725–734, 2011.

[99] W. W. Brennessel P. L. Holland R. Eisenberg Z. Han, L. Shen. *J. Am. Chem. Soc.*, 135:14659−14669, 2013.

[100] A. L.; Thomas R. J.; Fanwick P. E.; Walton R. A. Leeaphon, M.; Ondracek. *J. Am. Chem. Soc.*, 117:9715–9724, 1995.

[101] H. Chang T. Kouyama T. Katoc M. Kato T. Ohba, A. Kobayashi. *Dalton Trans.*, 43:7514–7521, 2014.

[102] D.; Su Z.; Shao K.; Zhao Y. Wang, Y.; Zhu. *Acta Crystallographica, Section C: Crystal Structure Communications*, 64:70–72, 2008.

[103] J.; Garcia-Vazquez J. Arturo; Luz D. M.; Casanova I.; Sousa A. Sousa-Pedrares, A.; Romero. *Dalton Transactions*, 7:1379–1388, 2003.

[104] G.; Naik H. S. Bhojya; Prabhakara M. C.; Vishnuvardhan T. K. Sreekanth, B.; Krishnamurthy. *Synthesis and Reactivity in Inorganic, Metal-Organic, and Nano-Metal Chemistry*, 40:955–962, 2010.

[105] O. L.; Nogueira V. M.; Santos R. H. A.; Gambardella M. T. P.; Lechat J. R.; Filho M. F. J. Mauro, A. E.; Casagrande Junior. *Polyhedron*, 12:297–301, 1993.

[106] B. N. Harum M. Volpe K. Gatterer F. Belaj N. C. Mösch-Zanetti G. Nuss, G. Saischek. *Inorg. Chem.*, 50:1991–2001, 2011.

[107] A.J.P. White D.J. Williams A.F. Hill, G.R.Owen. *Angew. Chem. Int. Ed.*, 38:2759–2761, 1999.

[108] B. N. Harum M. Volpe K. Gatterer F. Belaj N. C. Mösch-Zanetti G. Nuss, G. Saischek. *Inorg. Chem.*, 50:12632−12640, 2011.

[109] B. N. Harum G. Saischek F. Belaj N. C. Mösch-Zanetti G. Nuss, A. Ozwirk. *Eur. J. Inorg. Chem.*, 29:4701–4707, 2012.

[110] C. Gwengo S. V. Lindeman J. R. Gardinier, R. M. Silva. *Chem. Commun.*, page 1524–1526, 2007.

[111] Nuss G. *unpublished.*

[112] W. Wozniak C. Postmus, J.R. Ferraro. *Innorg. Chem.*, 6:2030–2032, 1967.

[113] Wells A. F. *Structural Inorganic Chemistry (5th ed.)*, Oxford Science Publications:ISBN 0–19–855370–6, 1984.

[114] A.; Castillo O.; Zamora F. Delgado, S.; Gallego. *Dalton Trans.*, 40:847−852, 2011.

[115] G. M. Sheldrick. *Acta Cryst.*, A64:112–122, 2008.